NAVAL POSTGRADUATE SCHOOL
Monterey, California

THESIS

SIX DEGREE OF FREEDOM MOTIONS OF TOWED SHIPS IN SHORT CRESTED SEAS

by

Errol Mac Glenn

September 2002

Thesis Advisor: Fotis A. Papoulias

THIS PAGE INTENTIONALLY LEFT BLANK

REPORT DOCUMENTATION PAGE			Form Approved OMB No. 0704-0188
Public reporting burden for this collection of information is estimated to average 1 hour per response, including the time for reviewing instruction, searching existing data sources, gathering and maintaining the data needed, and completing and reviewing the collection of information. Send comments regarding this burden estimate or any other aspect of this collection of information, including suggestions for reducing this burden, to Washington headquarters Services, Directorate for Information Operations and Reports, 1215 Jefferson Davis Highway, Suite 1204, Arlington, VA 22202-4302, and to the Office of Management and Budget, Paperwork Reduction Project (0704-0188) Washington DC 20503.			
1. AGENCY USE ONLY *(Leave blank)*	**2. REPORT DATE** September 2002	**3. REPORT TYPE AND DATES COVERED** Master's Thesis	
4. TITLE AND SUBTITLE Six Degree of Freedom Motions of Towed Ships in Short Crested Seas			**5. FUNDING NUMBERS**
6. AUTHOR Errol Mac Glenn			
7. PERFORMING ORGANIZATION NAME(S) AND ADDRESS(ES) Naval Postgraduate School Monterey, CA 93943-5000			**8. PERFORMING ORGANIZATION REPORT NUMBER**
9. SPONSORING / MONITORING AGENCY NAME(S) AND ADDRESS(ES) N/A			**10. SPONSORING / MONITORING AGENCY REPORT NUMBER**
11. SUPPLEMENTARY NOTES The views expressed in this thesis are those of the author and do not reflect the official policy or position of the Department of Defense or the U.S. Government.			
12a. DISTRIBUTION / AVAILABILITY STATEMENT Approved for Public Release; Distribution is Unlimited.			**12b. DISTRIBUTION CODE**

13. ABSTRACT ***(maximum 200 words)***

The scope of this thesis is to investigate the vertical and horizontal plane motions of surface ships in close proximity towing in irregular waves. Strip theory calculations have been utilized in order to predict the hydrodynamic coefficients and wave exciting forces and moments in sway and yaw, heave and pitch. The appropriate matching conditions between the two ships are provided in terms of the resistance-speed characteristics of the leading ship. The two-parameter Bretschneider spectrum with a cosine-squared spreading function is used to model the sea state environment. An extensive set of parametric studies is presented in a wide variety of developing and decaying sea states.

14. SUBJECT TERMS Close-Proximity Towing, Ocean Waves, Hydrostatics, Hydrodynamics, Ship Response, Wave Spectra, Slice, Kaimalino, SWATH, Bretschneider	**15. NUMBER OF PAGES** 81
	16. PRICE CODE

17. SECURITY CLASSIFICATION OF REPORT	**18. SECURITY CLASSIFICATION OF THIS PAGE**	**19. SECURITY CLASSIFICATION OF ABSTRACT**	**20. LIMITATION OF ABSTRACT**
Unclassified	Unclassified	Unclassified	UL

NSN 7540-01-280-5500 Standard Form 298 (Rev. 2-89)
Prescribed by ANSI Std. 239-18

THIS PAGE INTENTIONALLY LEFT BLANK

Approved for public release; distribution is unlimited

SIX DEGREE OF FREEDOM MOTIONS OF TOWED SHIPS IN SHORT CRESTED SEAS

Errol Mac Glenn
Lieutenant, United States Coast Guard
B.S., U.S. Merchant Marine Academy, 1997

Submitted in partial fulfillment of the
requirements for the degree of

MASTER OF SCIENCE IN MECHANICAL ENGINEERING

from the

NAVAL POSTGRADUATE SCHOOL
September 2002

Author: Errol Mac Glenn

Approved by: Fotis A. Papoulias, Thesis Advisor

Young W. Kwon, Chairman
Mechanical Engineering Department

THIS PAGE INTENTIONALLY LEFT BLANK

ABSTRACT

The scope of this thesis is to investigate the vertical and horizontal plane motions of surface ships in close proximity towing in irregular waves. Strip theory calculations have been utilized in order to predict the hydrodynamic coefficients and wave exciting forces and moments in sway and yaw, heave and pitch. The appropriate matching conditions between the two ships are provided in terms of the resistance-speed characteristics of the leading ship. The two-parameter Bretschneider spectrum with a cosine-squared spreading function is used to model the sea state environment. An extensive set of parametric studies is presented in a wide variety of developing and decaying sea states.

.

THIS PAGE INTENTIONALLY LEFT BLANK

TABLE OF CONTENTS

THIS PAGE INTENTIONALLY LEFT BLANK

LIST OF FIGURES

THIS PAGE INTENTIONALLY LEFT BLANK

LIST OF TABLES

THIS PAGE INTENTIONALLY LEFT BLANK

I. INTRODUCTION

The ocean waveform is an undulating process that transmits energy thousands of miles both efficiently and effectively. A twelve-second periodic wave group will take forty-eight hours to cross 1,000 miles of deep, open ocean with little loss of energy. When its power is unleashed on a rigid body, it becomes one of the greatest fears of all mariners and maritime insurance companies alike. It is the effort of the naval architect to design ships that can surpass a broad spectrum of waveforms and the energy associated with them.

A ship advancing at a relatively constant forward speed with an arbitrary heading in a train of regular waves will move in six degrees-of-freedom (three translational: surge, heave, sway; three rotational: pitch, roll, yaw). In order to be able to compute all responses of the vessels to random seaways, it is necessary to deal with the complete motions of the vessel in all six degrees-of-freedom, with special attention to the important couplings of heave and pitch, sway and yaw. For such a rigid body, six nonlinear equations of motion, with six unknowns, must be set up and solved simultaneously. In the case of a vessel of port/starboard symmetry and restrained about this axis of symmetry, the six non-linear equations can be reduced to two sets of three linear equations.

Specifically, it is the effort of this thesis to present a linear theory of ship motions. While most vessel responses are nonlinear to some extent, however, where nonlinearities are small a linear theory will yield reasonable predictions. Experimental and theoretical investigations have repeatedly shown that a linear theory analysis gives excellent predictions over a wide variety of sea states and vessel platforms (Beck).

A. MOTIVATION

Since the advent of steam, the level of engineering necessary to keep ocean-going vessels afloat and righting has had to become more and more complex. The economic demand of trading nations, and the warship designs of international navies continually pushes the complexity level to yet another extreme. Since the rapid developments in hydrodynamic theory of the 1950s, the advances in oceanography and computer technology have enveloped the marine engineers task in pursuing advanced designs in high-speed hull forms, and unusual platforms such as SWATH vessels.

Close proximity towing of surface ships is a matter of interest to the U.S. Navy and the Office of Naval Research. Several possible applications have been suggested including the SLICE/KAIMALINO connection (Nash) and the SEA LANCE configuration (TSSE). Of primary concern in this dissertation is the evaluation of motions in six degrees-of-freedom of the two ships when in close proximity towing operations.

II. WAVE SPECTRA

A. EARLY WAVE THEORY

Franz Gerstner of Czechoslovakia officially documented the first, rather primitive wave theory in 1802. He described how water particles move in oscillatory motions within the wave. He further described how the water particles in the crest move in the direction of wave advance and those in the trough move in the opposite direction. Such observations had been made centuries earlier; it was his discovery, however, that described the circular path of the water particles to have a diameter equal to the height of the passing wave (path diameter proportional to water depth). He essentially described a trochoidal wave (Figure 1). This discovery bridged the gap between the casual seafarer's observation to that of mathematical derivation and hence the theoretical beginning of hydrodynamics.

Following the theoretical came the experimental. The first experimentalists developed controllable wave tanks with the capability to reproduce waveforms over and over, and whereby careful measurements could be taken. Then in the 1950's a new breed of experiment was developed harnessing modern computations and statistical applications; and, hence, the numerical wave tank was born.

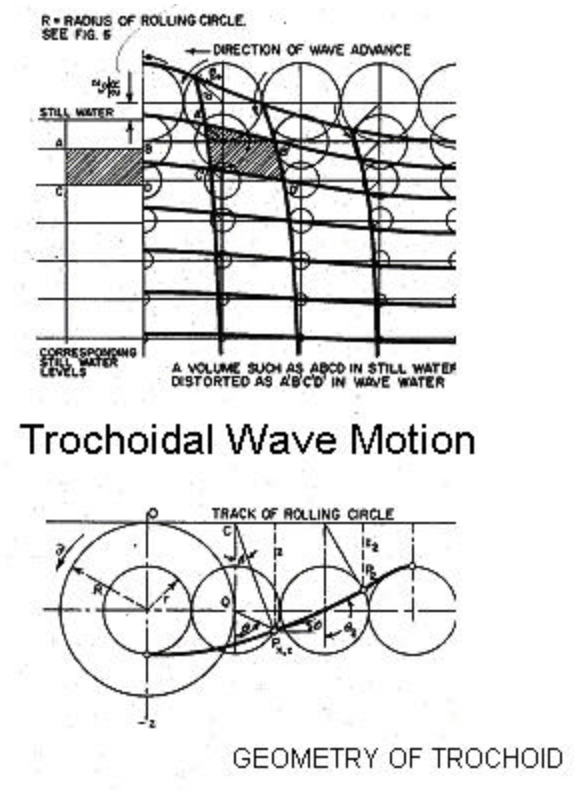

Figure 1. Trochoidal Wave (After Beck)

B. WAVE SPECTRA ANALYSIS

The understanding of vessel response at sea, and the ability to predict their behavior begins with the study of the nature of ocean waves in which the vessels will operate. Consequently, in order to understand the behavior of ocean waves, one must first understand their origin. Waves are a natural phenomenon that occurs between the interface of any two fluids of different density. While any kind of disturbance in the ocean will generate waves of sparing severity, there exist four primary sources: wind, earthquakes, landslides, and the gravitational attraction of the moon and sun. Of the four, the greatest of importance is the wind-generated waves. The size and variety of these wind waves depends on many factors, namely, the velocity of the wind, the distance it blows across the water, the time duration that it blows, and the depth of water in which the wind transverses (Figure 2). The character and signature of the wave is quickly lost as the wind energy is transferred to tidal energy in this highly stochastic ocean media. Once the winds have transferred their energy to the ocean surface, the waves begin their natural procession from the generation area. The original wind waves eventually decay, evidenced by the crests as they become lower, and more rounded and symmetrical. These crests then begin to move in groups of similar period and wave height, and their form becomes more and more sinusoidal. This origination theory becomes now the basis for our analytic discussion: sinusoidal wave forms moving as steady-state, constant parameter wave "trains" under the control of gravity and inertia; and their subsequent influence on sea-going vessels in-tow.

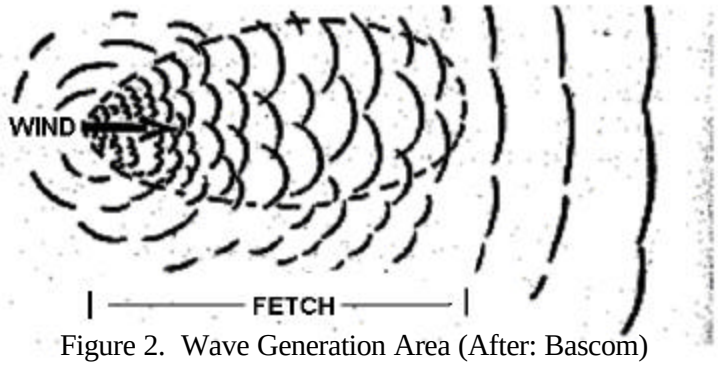

Figure 2. Wave Generation Area (After: Bascom)

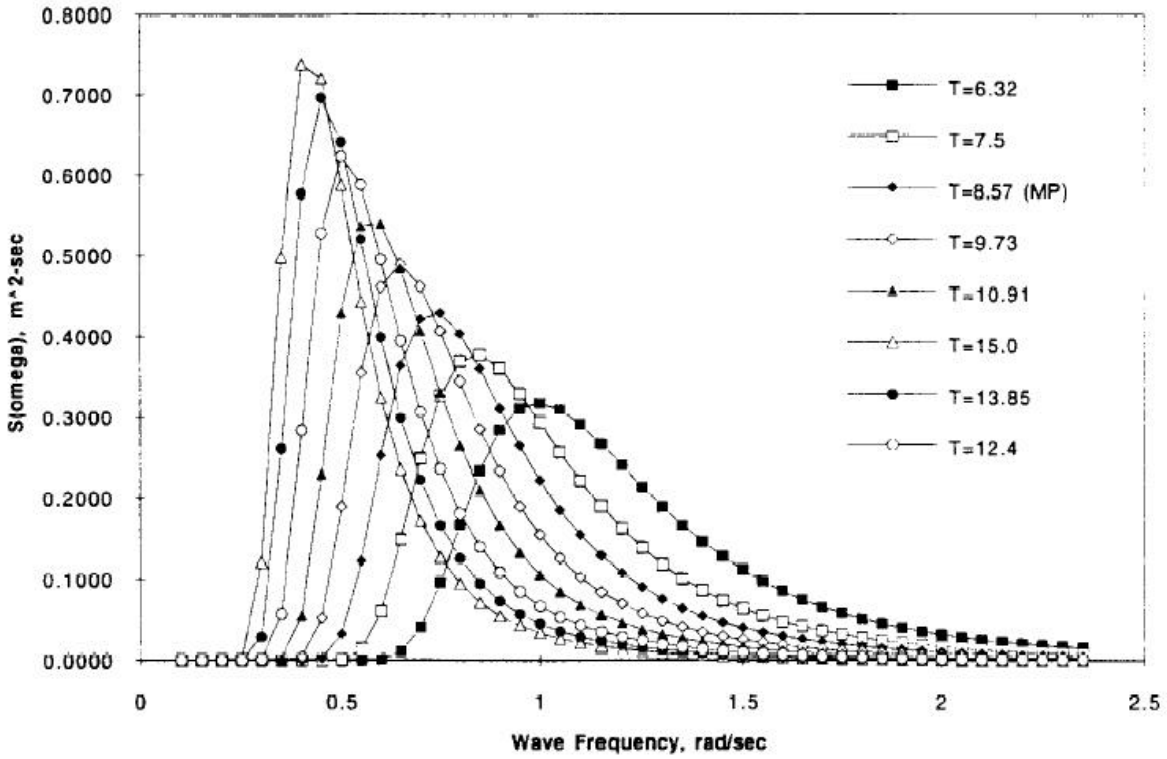

Figure 3. Sea State Four (Varying Period) (From: McCreight)

Waves are classified according to their period, which can range from a fraction of a second to more than ten thousand seconds. They can range in size from a ripple to great storm waves and tides whose wavelength can reach half the circumference of the earth (Bascom). Essentially we are studying a medium whereby the wave spectrum ranges from waves so small they can barely be seen to waves so long that they are not even noticed. For these extreme conditions our vessel design is safe. It is a narrow band of wave spectrum that can cause greatest damage to seagoing vessels and is of utmost concern to the naval architect and our research.

The energy in the ocean is distributed among several distinct groups of waves each with a defined range of periods (Figure 3). All waves can be classified as gravity waves since once they are started; gravity is the driving force that keeps these sea crests moving in a never-ending attempt to restore the original flat sea surface. The potential energy of each wave is due in part to the waves profile which consists of two sides of the equilibrium position: the crest that rises above datum sea line, and the trough that extends below. A wave group moves perpetually attempting to overtake the trough ahead

and restore equilibrium, suffering of course from the wave ahead with the same intent. For swell, the wave's potential and kinetic energies are equal. The kinetic energy possessed by a wave is due to the imparted motion of the water particles, while the remainder of the waves energy is the potential energy due to the elevation of the center of gravity of the mass of water in the crest above mean sea level (Figure 4).

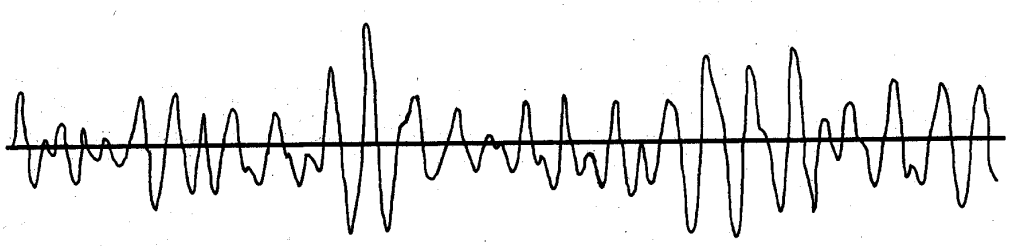

Figure 4. Point Spectra (Buoy Vertical Displacement vs. Time) (From: Beck)

Another classification of waves, although when fully developed act like gravity waves, are called capillary waves (short crested seas). They are a special waveform whose driving force is not gravity, but rather the surface tension at the water/wind interface. The capillary force is stronger than gravity, and given the open ocean condition, thrives in producing the most abundant kind of wind-generated wave. Capillary waves give rise to the development of ripples (incident wind drag), which are at the lower end of the wave spectrum, but none-the-less lead to the growth and overall combined effect of fully developed seas (wave energy absorption proportional to wind velocity).

Open ocean waves do not have the normal and precise properties as those generated in a wave generator. The height of the crests and the depths of the troughs are highly irregular. The theoretical terminology of a discernable wave period and wave velocity (celerity) is lost when taken to the real and observable, highly stochastic and irregular environmental oceanic swirl. For these very reasons is why the physics of ocean waves must rely on statistical methods in order to describe the properties of waves (Appendix B).

Wave heights, while apparently just as irregular, can be referenced to a datum line also referred to as mean sea level. Using mean sea level as a baseline, a sea state is

simply the result of superimposing a number of sinusoidal wave trains one on top of the other (Figure 5).

Each layer represents a series of regular sine waves, each having their own distinct wave height, wavelength, and direction; and coincides with the theoretical notions exactly. The summation of the wave crests and troughs of varying amplitude tend to cancel each other out, and conversely, amplify the local maximum or minimum depending on coincidence of discrete wave points throughout the ocean surface. Again, as these waves transverse each other, the cancellation and amplification will subside quickly as these respective wave groups transverse their own direction. Accordingly, the greater the number of wave layers the more random the sea surface.

The seemingly random nature of ocean waves can be better characterized by its energy spectra. This methodology assigns a value to the square of the wave height for each frequency and direction. Then, using statistical methods, the wave spectrum can be analyzed to reveal how the wave energy is distributed among various wave periods.

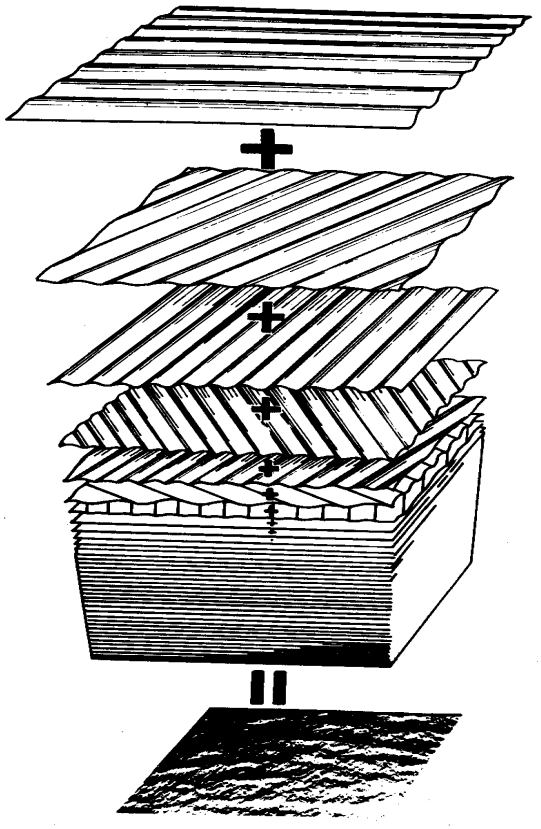

Figure 5. Wave Fourier Composition (From: Ochi)

The essential feature of these mathematical techniques/models is the concept of a spectrum defining the distribution of energy among the different hypothetical regular wave components having various frequencies (wave lengths) and directions. It has been formulated that the irregular motions of a ship in a seaway can be better described as the linear superposition of the responses of the same ship to all the wave components of the seaway. For our purposes, the linear theory assumption, as applied to the SWATH vessels, implies the vessels' response is described by the same statistical properties of a random (stochastic) surface wave environment. Given these assumptions, these surface waves can be characterized as having a Gaussian, or normal, probability distribution about some mean (zero amplitude, calm seas), under short-term statistically stationary conditions (Figure 4). This statistical technique will greatly simplify the numerical involvement of our study with regards to the application of statistics, probability theory and Fourier analysis techniques.

During the energy transfer between wind and water, there are several important wave interactions and wave-breaking processes that affect the dispersion and propagation of waves from the storm area. Particularly for the case of short crested, small amplitude waves, the principle of linear superposition applies. For example, if $\lambda_1(x_1,y_1,t_1)$ and $\lambda_2(x_2,y_2,t_2)$ are two wave systems, then $\lambda_1(x_1,y_1,t_1) + \lambda_2(x_2,y_2,t_2)$ is also a wave system. Inherent to this assumption, the two systems can move through each other without damping the other whereby all wave energy is conserved linearly. Of equal conceptual concern is wave celerity, or velocity, which is wholly a function of wavelength (shorter waves travel slower than longer waves). Referring to Figure 5, it can be shown that any wave system can be divided into a sum of component regular waves of various wavelength, amplitude and direction using Fourier Integral techniques. Since water is considered to be incompressible, the average value of vertical displacement at any instant for a sinusoidal, or regular, wave period is zero. While the mean will give us little statistical information, the variance, however, is a positive value that will directly relay the severity of the sea. A fundamental theory of statistics states that the variance of the entire system is determined by measuring the amount of variability in the distribution of the independent wave groups themselves. In general, the variance of a continuous function can be expressed by the following:

$$\langle x(t)^2 \rangle = \lim_{T \to \infty} \frac{1}{T} \int_{-T/2}^{T/2} z^2(t) dt \quad (1)$$

And in the case of simple harmonic sine waves, the variance of wave elevation of a single cycle is equal to one-half the square of the wave amplitude.

The slight errors involved in the assumed sinusoidal wave shape of linear harmonic wave theory are standard practice, and can be considered reasonable assumptions with little consequence. The errors only become significant when dealing particularly in the wave breaking phenomena, and when the geometry of the wave crests becomes unsteady. The correct mathematical analysis of linear short-crested irregular waves is formable with little error using short-term stochastic models of ocean waves.

Wave Properties (Two-Dimensional Waveform):

$$z(x, y, t) = \bar{z} \cos[k(x \cos b + y \sin b) - wt + e]$$

ε=phase angle

β=wave direction (global coordinates)

ω=wave frequency

Wave Number: $k = 2p / L_w = w^2 / g$

Wave Length: $L_w = 2p \frac{V_c^2}{g}$

Wave Period: $T_w = \left(\frac{2pL_w}{g} \right)^{1/2}$

Surface Profile: $z_0 = \bar{z} \cos k(x - V_c t)$

Velocity Potential: $f = -\bar{z} V_c e^{kz} \sin k(x - V_c t)$

Wave Variance: $\langle z^2 \rangle = 1/2 \, \overline{z^2}$

Wave Celerity: $V_c = \frac{L_w}{T} = \left(\frac{g}{k} \right)^{1/2}$ (Appendix B)

Continuing with the short-term model, the total wave system can be shown as a summation of many, if not infinite, independent wave components:

$$z(t) = \sum_i \overline{z}_i \cos(-w_i t + e_i) \quad (2)$$

This system can also be represented by a point spectrum, also known as a variance spectrum, S(ω) (the wave is observed only at a point, and none with respect to wave direction). At any particular wave frequency, ω_i, the variance of all the wave components within a small finite frequency band, $\delta\omega$, centered at ω_i is denoted by:

$$\left\langle z^2 \right\rangle \equiv S(w_i)dw \quad (3)$$

following:

$$\left\langle z^2 \right\rangle = 1/2\,\overline{z^2} \quad (4)$$

substituting:

$$1/2\,\overline{z^2} = S(w_i)dw \quad (5)$$

Integrating the RHS of the equation will resolve a good approximation of the wave system's total energy (Figure 3).

$$\overline{E} = \int_0^\infty S(w)dw \quad (6)$$

In the derivation of energy spectra in short crested seas, Figure 6 depicts only fourteen wave groups, a multi-directional short crested sea requires many more (73 was our approximation).

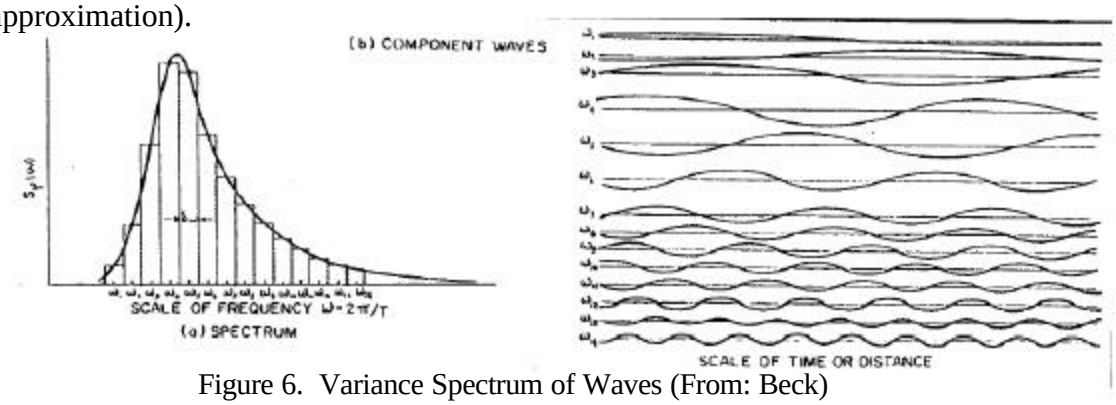

Figure 6. Variance Spectrum of Waves (From: Beck)

Figure 6, depicts several distinct sine curves of random phase. Numerical summing these will result in the irregular wave pattern in which we are interested. Figure 5 demonstrates this idea quite clearly.

While this seems a satisfactory depiction of the development of ocean wave spectra, and mathematically the variance, E, obtained from a point spectrum is a decent measure of the sea severity, it can be further shown that this measurement is still insufficient. A more complete characterization of the seaway must include wave component direction, also known as a directional spectrum. From the two-dimensional case to the three-dimensional case our generalized wave equation becomes:

$$z(x,y,t) = \sum_i \sum_j \overline{z_{ij}} \cos[k_i(x\cos b_j + y\sin b_j) - w_i t + e_{ij}] \quad (7)$$

and

$$\langle z(t)^2 \rangle \equiv E = \tfrac{1}{2} \sum_i \sum_j \overline{z_{ij}} = \int_0^\infty \int_0^{2p} S(w,b)\, db\, dw \quad (8)$$

Wave energy for a point has an angular distribution as well as a distribution over a range of frequencies. This angular distribution of wave energy is termed directional spreading and overall greatly increases the accuracy of our results when designing for short crested sea behavior. The directional spectrum thus defines the distribution of energy with even greater resolve defined by the frequency and direction of the variances of the individual wave system components (each having a unique combination of frequency and direction, and random phase angle). Furthermore, for our incorporated spreading function, the directional spectrum can be subdivided into the following:

$$S(w,b) = S(w)M(b) \quad (9)$$

where:

$$M(b) = \frac{2}{p}\cos^2 b \quad (10)$$

While the frequency and direction are accounted for, what is critical to our study is defining an idealized random seaway. We have already discussed the constructs of wave spectra from recorded data, but how can we reconstruct such data given certain

environmental parameters? This technique is particular to the design process, where we are only interested in recreating wave energy spectroscopy. This approach allows the designer to modify such environmental parameters incrementally to discern ship response to specific wave parameters.

The Bretschneider Spectrum was selected and can be presented as follows:

$$S(w) = \frac{1.25}{4}\frac{w_m^4}{w^5}H_s^2 e^{-1.25(w_m/w)^4} \quad (11)$$

$$w_m = \frac{2p}{T_m} \quad (12)$$

where:

T_m =input modal wave period

H_s=input significant wave height defined as the average one-third highest wave heights ($H_{1/.3}$)

This is a two-parameter wave spectrum and is a widely accepted design parameter for marine systems. Using this infamous two-parameter spectral formulation it is possible to generate a myriad of wave groups of varying severity and size composition. This spectral density function can quickly illustrate the magnitude of wave energy. The most commonly used definition of sea severity is significant wave height, which can be deduced from the wave spectrum as being equal to four times the square-root of the area under the curve (Figure 3).

Continuing with the linear theory assumption, the spectral density of any response can be found by multiplying the incident wave spectrum by the square of the response amplitude operator (RAO) of the desired response. In control theory, for example, the RAO is often called the transfer function of the linear system function. For any given frequency, the RAO is the amplitude and phase of the desired response to regular incident waves. Also known as the motion transfer function, the response amplitude operator (RAO) maps the complex response of a vessel to a seaway or input spectrum as a

function of frequency. The spectrum of the particular response that the RAO has been computed for is calculated from:

$$S_R(w) = \left|RAO(w)\right|^2 S(w,b) \quad (23)$$

In this equation, $S_R(w)$ is the response of the vessel to the input sea spectrum for a given frequency. Ship response then can be calculated for a given wave frequency and significant wave height. For example, the complex absolute motions predicted in regular wave modeling (? s, ?k) are converted into RAO's for absolution motion as

$$RAO(x_{s,k}) = abs(x_{s,k}) \quad (24)$$

The response spectrum for absolute motion then becomes:

$$S_{R\_x_{s,k}}(w) = \left|abs(x_{s,k})\right|^2 S(w,b) \quad (25)$$

Finally, all motion analysis speed polar plots are resolved in RMS values:

$$(RMS)^2 = \int_b \int_w S_R \, dw \, db \quad (26)$$

THIS PAGE INTENTIONALLY LEFT BLANK

III. SHIP RESPONSE

The longitudinal motions of a symmetrical ship with symmetrical moorings in regular waves can be considered distinctly from the horizontal degrees of motion. The principle modes are the heave and pitch degrees-of-freedom (modes 3 and 5, respectively). In particular, the cross coupling between these two modes is critical to the success of this model. To further this discussion, it has also been shown that the surge degree of freedom (mode 1), given the SWATH vessels' architecture, has only a minor contribution and can be neglected for the present discussion (refer: Conclusions pp.23) For the following derivation, the SLICE/KAIMALINO coupling is rigid, has constant forward velocity, and are resolved into the simplified head seas case (waves from the bow; $\mu=180^0$). It is also assumed that the wave excitation forces are linear and harmonic, acting according to the wave encounter frequency (*Doppler Shift*). Using the linear theory assumption, the responses of the vessel will be directly proportional to wave amplitude and the frequency of occurrence corresponds to the frequency of encounter.

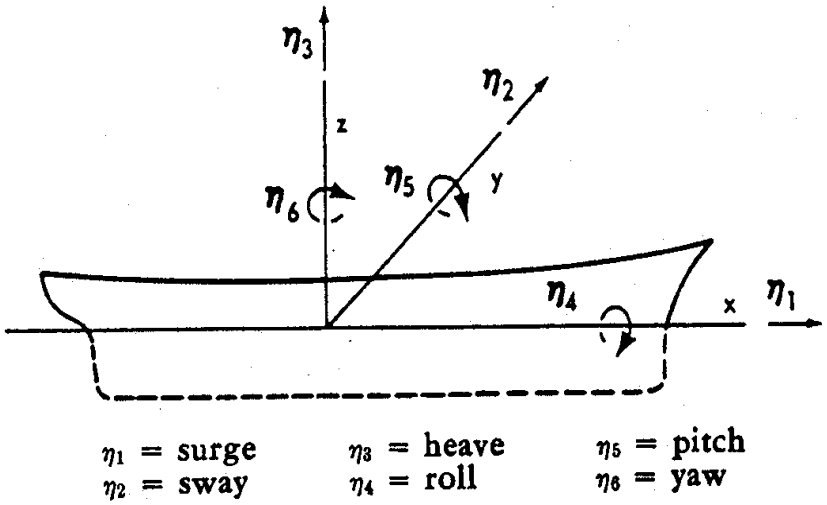

Figure 7. Degrees-of-Freedom for Ship Motions (From: Beck)

From Newton's second law of motion, a translational displacement is defined as the mass times the acceleration, therefore, for heave we have (center of gravity located at the waterline):

$$\Delta \ddot{h}_3 = F_3 \quad (27)$$

and for pitch, the rotational modes equal the mass moment of inertia times the angular acceleration:

$$I_{55} \ddot{h}_5 = F_5 \quad (28)$$

where Δ equals displacement, I_{55} is the mass moment of inertia about the y-axis and F_3 and F_5 are the total force and moment acting on the body.

For our discussion (linear theory), the total force and moment consist mainly of hydrostatic and hydrodynamic fluid forces:

$$F_3(t)=F_{ex3}(t)+F_{H3}(t) \quad (29)$$

and

$$F_5(t)=F_{ex5}(t)+F_{H5}(t) \quad (30)$$

where F_{ex} is the exciting force due to the waves acting on the restrained ship, and F_H is the radiation force due to ship motions in an assumed calm sea, ideal case. Again due to a linear theory assumption, the fluid forces can be divided as such.

$$F_{EX3}(t) = |F_{EX3}| \cos(w_e t + e_3) \quad (31)$$

$$F_{EX5}(t) = |F_{EX5}| \cos(w_e t + e_5) \quad (32)$$

where $|F_{EX3}|$ refers to the amplitude of the heave force and $|F_{EX5}|$ refers to the amplitude of the pitching moment. Also called the Froude-Krylov, or Korvin-Kroukovsky, excitations (NASH), these excitations represent the integration of the pressure field, over the ship wetted surface area, which would have existed in the incident wave system if the ship were not present. The diffraction excitation forces and moments, which are also a component of $|F_{EX3}|$ and $|F_{EX5}|$, are caused by the diffraction or modification of the

oncoming waveforms. The respective epsilon values are the phase angles between the excitation force and sea waves.

$$F_{H3} = [A_{33}(w)\ddot{h}_3 + B_{33}(w)\dot{h}_3 + C_{33}(w)h_3 + A_{35}(w)\ddot{h}_5 + B_{35}(w)\dot{h}_5 + C_{35}(w)h_5 \quad (33)$$

$$F_{H5} = [A_{53}(w)\ddot{h}_3 + B_{53}(w)\dot{h}_3 + C_{53}(w)h_3 + A_{55}(w)\ddot{h}_5 + B_{55}(w)\dot{h}_5 + C_{55}(w)h_5 \quad (34)$$

where A_{jk}-terms correspond to added mass in phase with vertical accelerations, the B_{jk}-terms to hydrodynamic damping in phase with vertical velocity, and the C_{jk}-terms to restoring forces (buoyancy effects) in phase with ship displacements. These coefficients were developed using a strip theory (a fast and reliable numerical method, capable of accommodating a wide range of hull forms). ($A_{35}(w)\ddot{h}_5$ represents the force in the heave mode due to an acceleration in the pitch mode.)

As may be evident to the reader, the coupled equations are similar in form to that of a two-degree-of-freedom mass-spring-damper system (added mass+mass, damping, and restoring terms on the LHS; excitation forces on the RHS). The dynamics of the two systems, however, are far from similar. For the ship system all coefficients and excitation forces are all functions of frequency, whereas for the simple mass-spring-damper system these values are time independent. While solutions to the vessel coupling problem are possible in the time domain, such methods require heavy mathematics involving complicated convolution integrals. In order to overcome this difficulty the problem need only be solved in the frequency domain. The exciting force, therefore, can now be defined in the frequency domain as:

$$F_{ex}(t)=F_{ex}e^{iw_e t} \quad (35)$$

Defining the motion and its derivatives:

$$\begin{aligned} h(t) &= \bar{h}e^{iw_e t} \\ \dot{h}(t) &= iw_e \bar{h}e^{iw_e t} \\ \ddot{h}(t) &= -w_e{}^2 \bar{h}e^{iw_e t} \end{aligned} \quad (36)$$

where $\overline{h_j}$ is the complex response amplitude containing both magnitude and phase of the response.

Finally, linearizing the equations of motions (Abkowitz, 1969), (note Figure 1):

$$
\begin{aligned}
&\Delta(\ddot{\hbar}_1 + \overline{z_c}\ddot{\hbar}_5) = F_1 \\
&\Delta(\ddot{\hbar}_2 - \overline{z_c}\ddot{\hbar}_4 + \overline{x_c}\ddot{\hbar}_6) = F_2 \\
&\Delta(\ddot{\hbar}_3 - \overline{x_c}\ddot{\hbar}_5) = F_3 \\
&I_{44}\ddot{\hbar}_4 - I_{46}\ddot{\hbar}_6 - \Delta\overline{z_c}\ddot{\hbar}_2 = F_4 \\
&I_{55}\ddot{\hbar}_5 + \Delta\{\overline{z_c}\ddot{\hbar}_1 - \overline{x_c}\ddot{\hbar}_3\} = F_5 \\
&I_{66}\ddot{\hbar}_6 - I_{64}\ddot{\hbar}_4 + \Delta\overline{x_c}\ddot{\hbar}_2 = F_6
\end{aligned}
\qquad (37)
$$

Rewriting the equation of motion in generalized form:

$$
\sum_{k=1}^{6}[-w_e^2(\Delta_{jk} + A_{jk}) + iw_e B_{jk} + C_{jk}]\overline{h_k} = F_j^I + F_j^D \qquad (38)
$$

IV. RESULTS

The following results (Table 1) are presented in speed polar plots (Appendix A). As discussed earlier, waves on the bow, or head seas, correspond to 180^{o} on the plots. The input parameters as necessitated by the Bretschneider Equation are modal period and significant wave height, with the additional input of connection ratio on behalf of vessel coupling to determine connection force and, ultimately, modal excitation. The radial coordinates range from zero to twenty knots, and all results show contours of constant connection force (RMS values).

Table 1. Numerical Test Matrix

Significant Wave Height	Modal Period	Connection Ratio		
5	5	0.1	0.5	1.0
5	10	0.1	0.5	1.0
5	15	0.1	0.5	1.0
10	8	0.1	0.5	1.0
10	12	0.1	0.5	1.0
10	16	0.1	0.5	1.0
20	8	0.1	0.5	1.0
20	12	0.1	0.5	1.0
20	16	0.1	0.5	1.0
30	12	0.1	0.5	1.0
30	16	0.1	0.5	1.0
30	20	0.1	0.5	1.0

Somewhat illusive to the discussion has been from where are such motions observed? Up to this point it has been assumed that the wave spectra has been with respect to some fixed referenced point. The absolute displacements, velocities, and accelerations have all been assumed to be with respect to an absolute or non-rotating/transversing observer. However, if the velocity of the wave groups along with the velocity of the vessel is taken into account the results will change significantly. The time record, or frequency of encounter, of a moving point relative to a moving fluid media and some global fixed inertia reference frame will undoubtedly be significantly affected by the *Doppler Shift* in the component frequencies of the wave system itself.

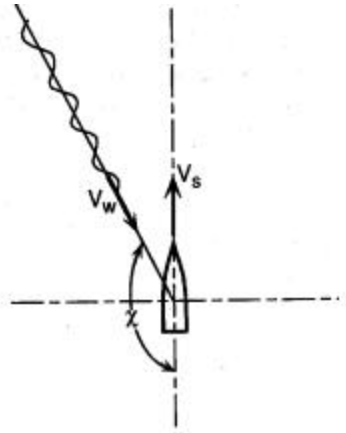

Figure 8. Frequency of Encounter (From: Ochi)

The location of the ship can be given by:

$$x_o = x + U_o t$$
$$y_o = y \quad (40)$$

Where the component $U_o t$ is the difference between the body fixed frame and the global coordinates. Substituting into the two-dimensional wave equation, the expression for the wave field as observed from the moving ship becomes:

$$z\,(x,y,t) = \overline{z}\,\cos[kx\cos m + ky\sin m - (w - kU_o\cos m)t + e] \quad (41)$$

From Figure 8 the frequency of encounter can then be described as:

$$T_e = \frac{l}{U_w - U_o\cos m} \quad (42)$$

$$w_e = \frac{2p}{l}(U_w - U_o\cos m) \quad (43)$$

$$= w_o - \frac{w_o^2}{g}U_o\cos m \quad (44)$$

$$w_e = w(1 - a) \quad (44)$$

For the simplified solution:

$\alpha<0$: bow waves, $\omega_e>\omega$

$0<\alpha 0.5$: stern waves $\omega_e<\omega$. (waves pass the ship quickly)

maximum ω_e when $\alpha=0.5$

$0.5<\alpha<1$: stern waves $\omega_e<\omega$ (waves pass the ship slowly)

$\alpha=1$: wave velocity equal to that of the ship.

$\alpha>1$: waves come from the stern, but the ship overtakes the waves so that the waves appear to actually come from ahead.

The change in frequency from that of oscillation to wave encounter is analogous to the *Doppler Shift* found in sound waves and electro-magnetic theory. Considering ahead seas, the frequency of encounter will be greater than that of the absolute frequency and is therefore another critical ingredient to the physics of vessel motion and overall understanding of our results. The frequency of encounter and according frequency shifts attributed to vessel velocity has a profound influence on ship motions. In particular, noting the circular, or concentric, motion amplitudes with high and low, and then high again motion amplitude results. These results are due in part to the speed-polar plot data representation. With zero velocity at the center, and increasing outwardly in integer intervals to a maximum velocity of twenty knots, the frequency shifts are rather evident. All statistical assumptions remain the same, as only the point of reference has changed; however, the directional spectrum must also be slightly modified to account for such said frequency shifts.

$$\left\langle z_e(t;U_o)^2 \right\rangle \equiv E = \tfrac{1}{2}\sum_i \sum_j \overline{z}_{ij}^{\,2} = \int_0^{\infty}\int_0^{2p} S(w_e, b)\, d\, b\, dw_e \quad (45)$$

Realizing the spectrum of encounter to be the limit as $d\,b\,dw$ tends to zero:

$$S[(w_e)_{ij}, b_j] = \tfrac{1}{2}\overline{z}_{ij}^{\,2} / dw_e db \quad (46)$$

such that:

$$dw_e = \left(1 - \frac{2wU_o \cos b}{g}\right) dw \quad (47)$$

solving:

$$S(w_e, b) = S(w, b)/[1 - (2wU_o / g)\cos b] \quad (48)$$

The null space on the plots is a combination of when α>1, and/or when the denominator for the spectrum of encounter is equal to zero (spreading function).

Table 2. Horizontal Force Comparison

Horizontal Force Differential (Connection-Ratio)						
Significant Wave Height	5	**0.1**	-28.60%	**0.5**	28.60%	**1.0**
	5	**0.1**	0.00%	**0.5**	20.00%	**1.0**
	5	**0.1**	-12.50%	**0.5**	28.60%	**1.0**
	10	**0.1**	-16.60%	**0.5**	16.60%	**1.0**
	10	**0.1**	-9.10%	**0.5**	27.30%	**1.0**
	10	**0.1**	-14.30%	**0.5**	33.30%	**1.0**
	20	**0.1**	-20.00%	**0.5**	20.00%	**1.0**
	20	**0.1**	-12.00%	**0.5**	12.00%	**1.0**
	20	**0.1**	-14.30%	**0.5**	33.30%	**1.0**
	30	**0.1**	-12.50%	**0.5**	12.50%	**1.0**
	30	**0.1**	-18.20%	**0.5**	18.20%	**1.0**
	30	**0.1**	-14.30%	**0.5**	14.30%	**1.0**

V. CONCLUSIONS AND RECOMMENDATIONS

A. CONCLUSIONS

The response of a ship advancing in a stochastic seaway is obviously a complicated phenomenon involving the distinct and recognizable interaction between hydrodynamic forces and vessel dynamics. Quantifying and measuring either sides of the equilibrium equation (39) may never be a perfect science, however, experiment and prediction prove theoretical insight is a must for advances in naval architecture. While the present discussion involves only distinct evidence for vessel response to waves of various, albeit steady, frequencies, we can subsequently still predict the statistics of the responses to actual random seaways.

The measured distribution of hydrodynamic forces along the length of the vessels (strip theory predictions) for lower frequencies (longer wavelengths) become greater and more adversely affected by the effects of three-dimensionality and forward speed. In all cases, lower wave periods have the greatest impact on the vertical and horizontal connection forces (on the order of 3.0). For higher frequencies the agreement between the strip theory approximation and experimentation are reasonably good for zero forward speed, but the agreement between theory and experiment diverges as the speed increases (Beck).

As can be seen by the speed polar plots, forward speed dependence is clearly visible in the numerical results. Pitch motion becomes very small in beam seas, but become most severe in head seas. The effects of wave frequency and forward speed in head seas have been illustrated. In general, a reduction in forward speed will reduce the heave and pitch motion in long wavelengths and increase the motion in short waves. The motions in short waves ($L/L<1.0$) are significantly less than in longer wavelengths. Vertical connection forces remained relatively the same for increases in the connection ratio varying only a maximum of 9.1%. Again, keeping all parameters constant and varying the connection ratio, the horizontal components on the other hand ranged from 0-33%. The most important results/parameters for seakeeping responses, and amplitude motion in random seas are wave period, wave amplitude (significant wave height), and

forward speed, and a weaker function of connection ratio for the ranges considered. These results compare with results found earlier (Okan), whereby the connection forces are not a monotonic function of the towline length (therefore, it is possible to select a towline length so that the connection force in minimized).

For the translational modes, the surge and heave motions were maximized in seas forward of the bow. Horizontal plane motions tended to be damped out while vertical plane motions grew larger with respect to speed for wave angles forward of beam. For sway, it was beam seas that excited the largest motions while yaw was greatest in quartering seas. Sway and yaw have no hydrostatic restoring forces displaying high amplitude motions in quartering and beam seas. The wave encounter frequencies are also much lower in quartering and following seas than in head seas or on the bow and evidently lead to larger amplitude sway and yaw motions.

It must be remembered that the incident and diffracted wave velocity potential's (39) (respective wave velocity potentials before and after contact is made with vessel) unsteady components are all higher order and are neglected in the derivation of excitation forces using the linear theory assumption. Viscous effects also play a more important role in the transverse modes than in the horizontal. For example, if the ship is at an apparent angle of attack and coincidently yaws relative to the ship's forward motion, viscous effects will undoubtedly come into effect at the bow. Significant transverse rotation, relative to angle of attach, will transpire. However such motions have not been incorporated into the ship motion algorithm. Additionally, surge motion is neglected due to the simplified head seas case where the vessel surges forward on the surface of the wave, also known as surfing. Completing the free-body-diagram on the vessel/wave interface, it is easy for one to picture the buoyancy force normal the wave face and opposing the vessel body weight component. The included angle between the normal force and the weight component is very small, none-the-less the included positive vector is a surge force and is clearly present. Sufficiently large tension values, however, may stabilize and counter such forces in the coupled two-vessel system

Continuing with our discussion, for very long waves the heave motion amplitude approaches the wave amplitude and the pitch amplitude is the same as the maximum wave slope for such conditions where the vessel moves with the waves (planar motion) resulting in lower transverse forces. As the ships are modeled in-tow, they move together similarly at the corresponding connection points as a result of the coupling connection. As the connection ratio decreases, the leading and trailing ship motions become closely matched as the towline length is reduced, while some variation is observable for larger towline lengths. Furthermore, the horizontal connection force becomes larger for towing lengths ($l/L>0.1$), while the vertical force decreases (of varying inconsistent magnitude). Additionally, there is no clear dependence of the connection force and consequent ship motions due to forward speed, there is a large variation with no evident trend.

The complexities of wave resistance, incident waves and associated singularities (wave breaking), as well as some of the nonlinearities associated with the free surface problem tend to make the speed polar plots appear more as a glimpse into the amplitude motions of six degrees rather than absolute. While the most advanced present-day techniques are beyond the capacity of modern-day computers, and will likely be the case for years to come, perhaps the simplex method describe here will offer a numerical breach into the many unknowns and possibilities of ship response to random impulses. In fact, in the open ocean, the evolution and development of waves from ripple to sea state ten is likely never to be observed given the obvious explanation that the wave source is, in fact, rarely an impulse. Although in a physical sense the ocean wave and its multiple sea states cannot be reproduced in a laboratory, from a mathematical standpoint this is quite feasible. "In fact, the theoreticians have become so bold as a result of the success of their complicated equations that there is danger the study of waves will fall entirely into the hands of those who have never [even] been to sea." (Bascom)

B. RECOMMENDATIONS

The overall effect of vessel control must be realized in order to better determine the surge and roll motion amplitudes. Surge is severely affected by propeller thrust, rudder design, and steering gear response. Propeller response and the unsteady wake behind SLICE would either serve to dampen or excite mode amplitudes for the KAIMALINO. Furthermore, the idealized mechanical linkage between the two vessels is a major contributor to the coupling mechanics between the vessels and correlates directly to roll motion. The damping arising from wave making due to roll is very small for this mode; while for heave, yaw, sway, etc. it is a major contributor. This idealized linkage assumption, however, should be altered to incorporate a more realistic damping/excitation force when considering the roll motion.

Numerically, the boundary conditions on the hull and on the free surface both contained terms based on the steady perturbation potential. In trying to solve this boundary value problem, it is determined that there exists an interaction between the steady and unsteady components of this potential. Addressing the nonlinearities associated with the potential function, in particular, the velocity squared term in the pressure/Bernoulli equation and viscous (damping) effects. Similarly, the smooth free surface assumption should be reconsidered (incident wave brake). Unique solutions of the Laplace equation (Appendix B) require boundary conditions on all surfaces surrounding the fluid domain. The major nonlinearities in the general potential flow problem are in the free-surface boundary conditions that involve the square of the fluid velocities and products of these velocity terms with the unknown free-surface amplitude. This potential flow problem still is quite difficult and further underlying assumptions will be necessary. For our simplifying assumption of linear theory, the interaction was considered negligible and only the free-stream value was deemed necessary. Although many in the hydrodynamics field practice this assumption; is this a reasonable hypothesis considering our significant wave heights and varying ship velocities?

Any disturbance of the water surface, including the passage of a ship, produces waves. Much of the power expended in propelling the ship goes into such said wave-

making processes and while this is a prime concern of the marine engineer in the interest of inefficiencies and power losses, it may also be of interest to future proceedings and research into using SWATH vessels in-tow. As the ship passes through the water it is accompanied by at least three different pressure disturbances on each side, which produce several distinct wave trains in consistent order, direction, and symmetry. Lord Kelvin investigated the pattern of waves generated by an idealized pressure disturbance concentrated at a point and moving in a straight line. The Kelvin wave pattern, as it is called, is characterized by (1) diverging waves (a series of curved crests, concave outward and lying in echelon position); (2) transverse waves (convex forward and perpendicular to the direction of motion); (3) crest intersections (where the diverging and transverse waves coincide). It is this trailing pattern that should be further researched and incorporated into the two-vessel design. The Volex wave system (ship applications as apposed to point disturbance) and pressure deductions should be determined for the SLICE twin hull configuration. Do the resultant stern waves contribute to the overall wave resistance? When considering the positive pressure wave at the stern, should this attribute to added resistance and be incorporated into the connection force?

Finally, should a more realistic six degree-of-freedom coupling be developed, the potential to model this result at the Fleet Numerical Oceanographic Center (FNOC), Monterey, CA, in real-time has been addressed to FNOC, and may better ascertain the feasibility and validity of the coupling algorithm. (Virtually place the SLICE/KAIMALINO coupling anywhere in the world.)

Anecdotal:

With the advantages of the computational domain come the disadvantages. It has been found, without careful observation numerical waves can reflect from the boundary conditions and return to and interfere with initial conditions fouling results (Beck and Reed, 2001).

"To impact ship design, computational methods must be integrated into the design process. This in turn means that the computer codes must be fast enough that they can provide results in no more than an hour or two of computing time. While there has been work done on improving the computational efficiency of computer codes for ship hydrodynamics problems, a tremendous amount of work still needs to be done. The work to date on computational efficiency has resulted in a large enough literature base that this subject is worthy of a paper of its own; time and space [and money] obviously preclude this." (Beck and Reed, 2001).

APPENDIX A. SPEED POLAR PLOT RESULTS

Considering the limited memory presently allocated to MS WORD, only a small sampling (20 modal solutions) of the 360 member set will be included to illustrate the numerical results. If further detail is required of the results outlined in Table 1, please email Professor Fotis Papoulias (papoulias@nps.navy.mil), Mechanical Engineering Department, Naval Postgraduate School; Monterey, CA.

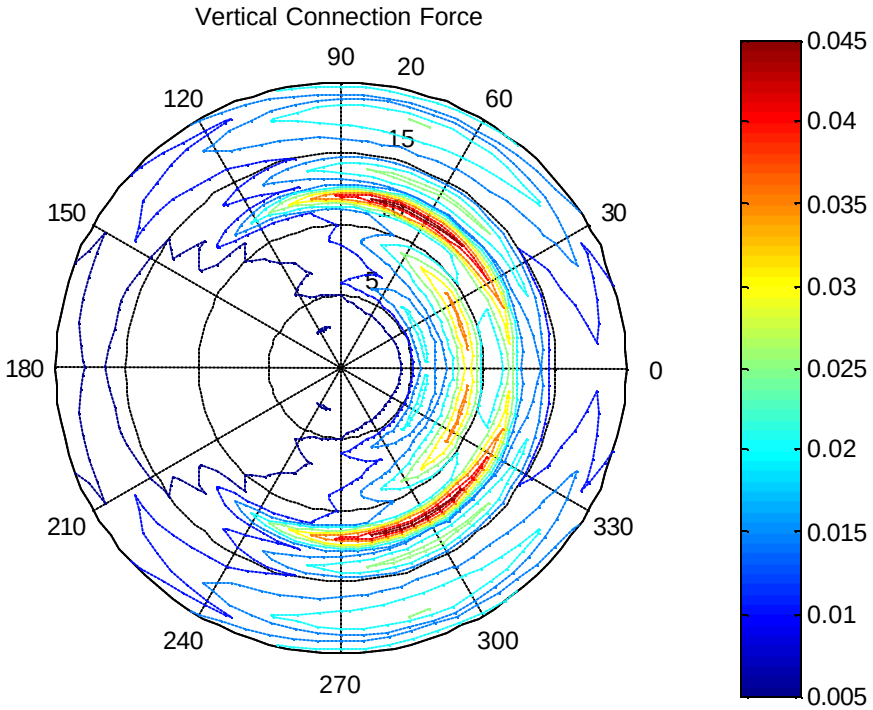

Figure A-1. Vertical Connection Force (HS: 5 feet, T_m: 5 sec., l/L: 0.1)

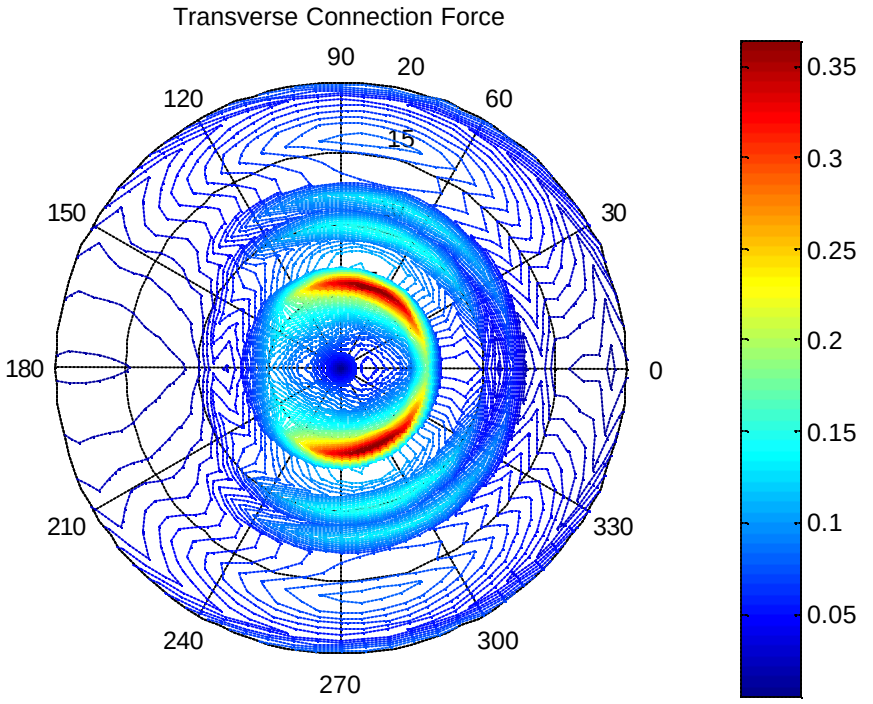

Figure A-2. Transverse Connection Force (HS: 5 feet, T_m: 5 sec., l/L: 0.1)

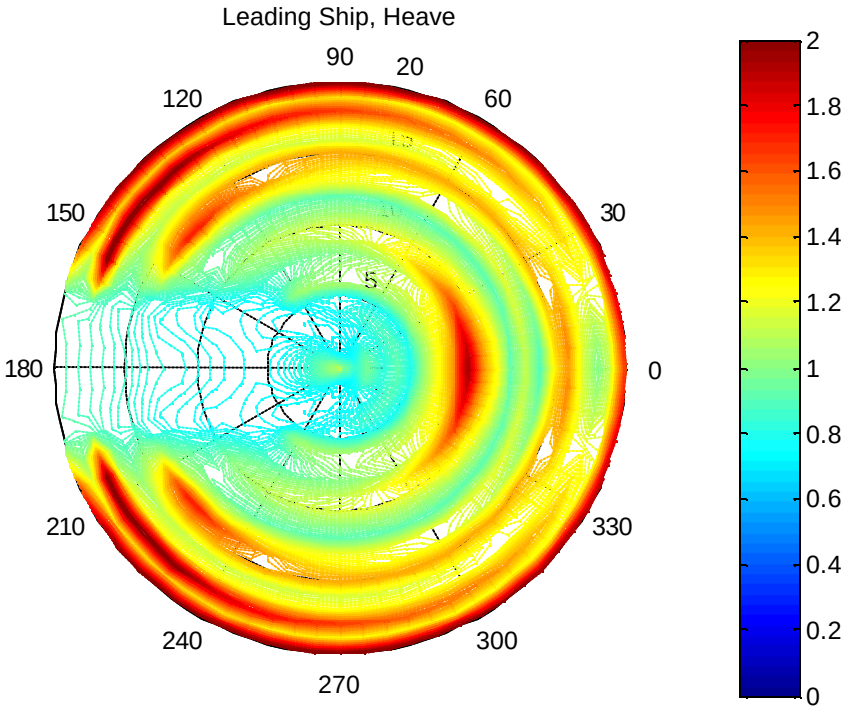

Figure A-3. SLICE Heave Amplitude Motion (HS: 5 feet, T_m: 5 sec., l/L: 0.1)

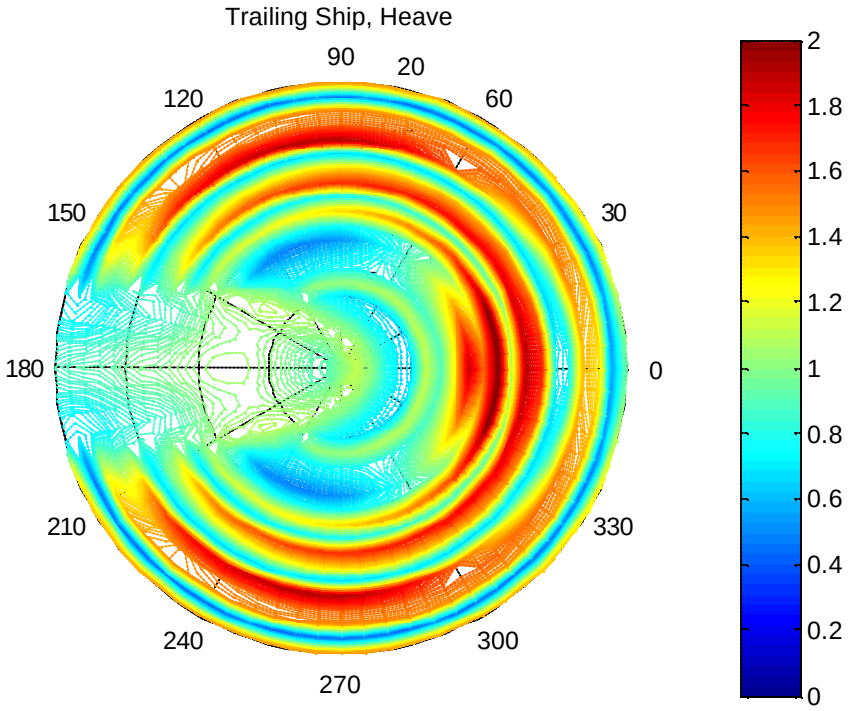

Figure A-4. KAIMALINO Heave Amplitude Motion (HS: 5 feet, T_m: 5 sec., l/L: 0.1)

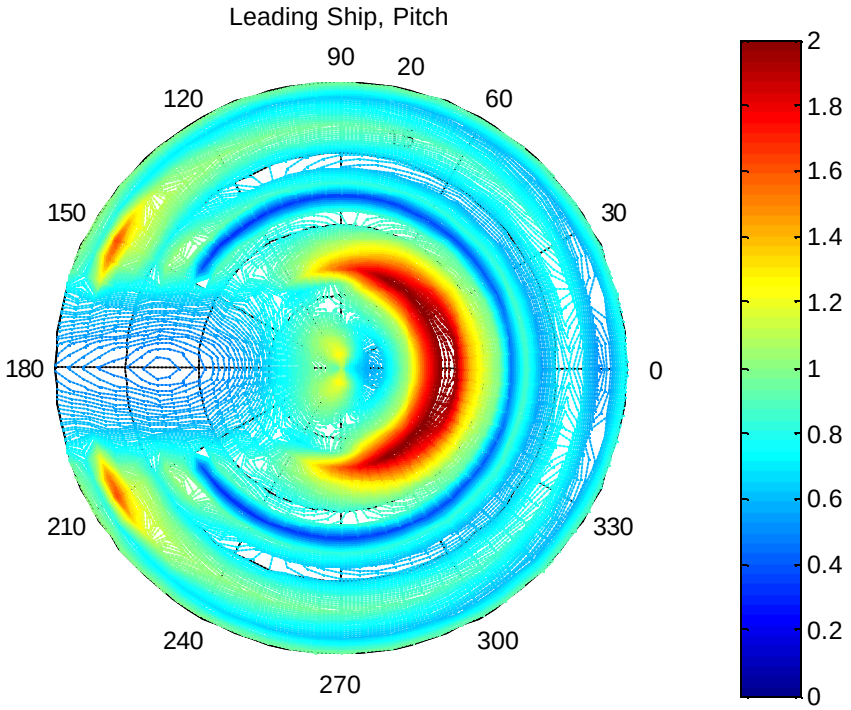

Figure A-5. SLICE Pitch Amplitude Motion (HS: 5 feet, T_m: 5 sec., l/L: 0.1)

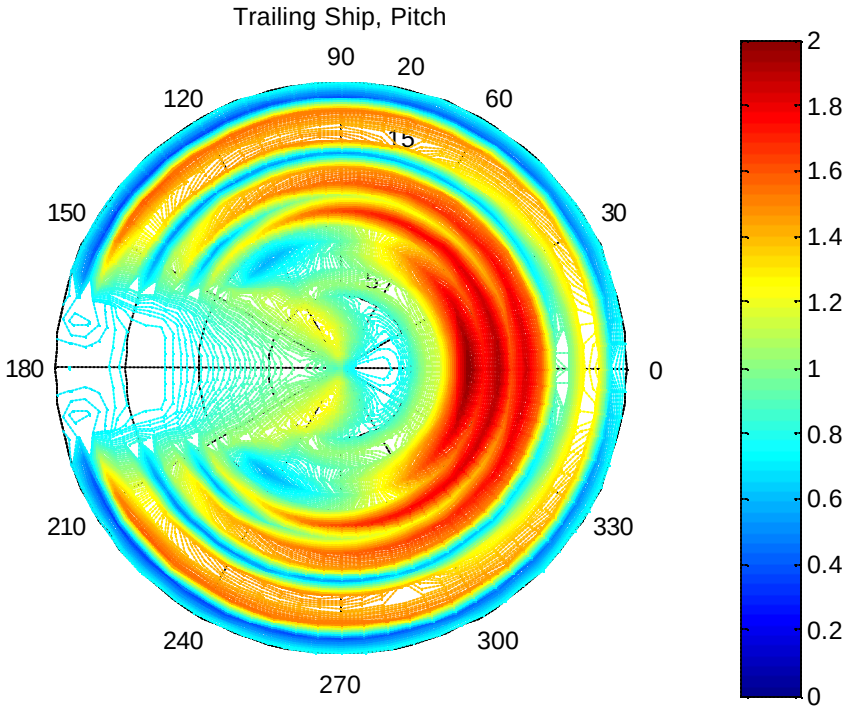

Figure A-6. KAIMALINO Pitch Amplitude Motion (HS: 5 feet, T_m: 5 sec., l/L: 0.1)

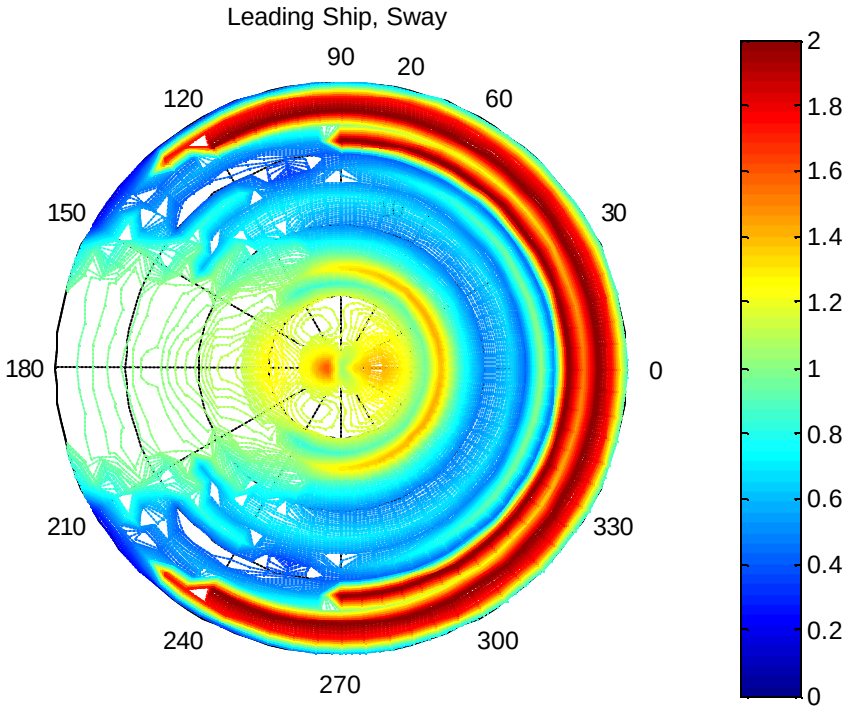

Figure A-7. SLICE Sway Amplitude Motion (HS: 5 feet, T_m: 5 sec., l/L: 0.1)

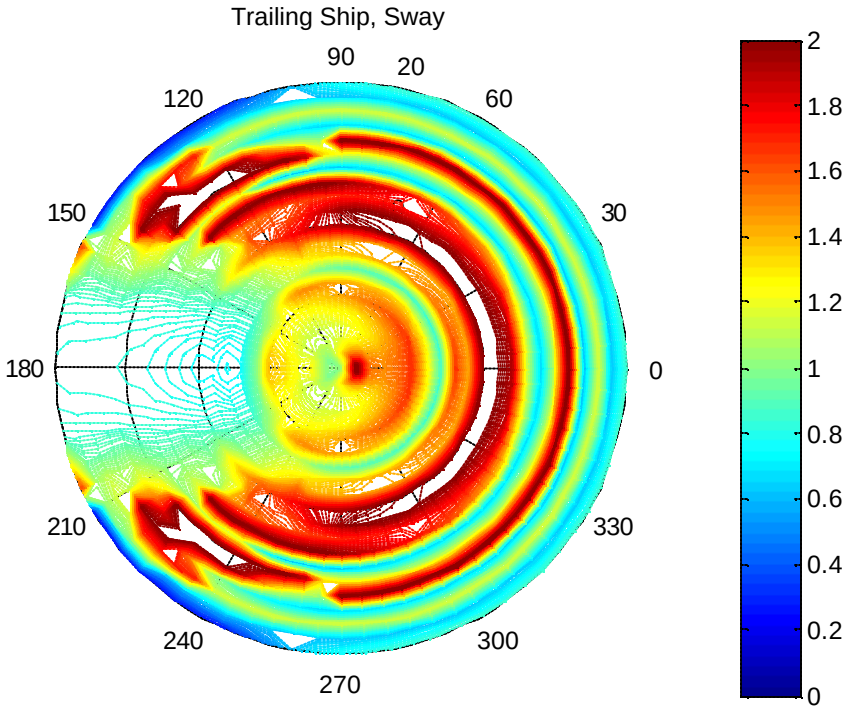

Figure A-8. KAIMALINO Sway Amplitude Motion (HS: 5 feet, T_m: 5 sec., l/L: 0.1)

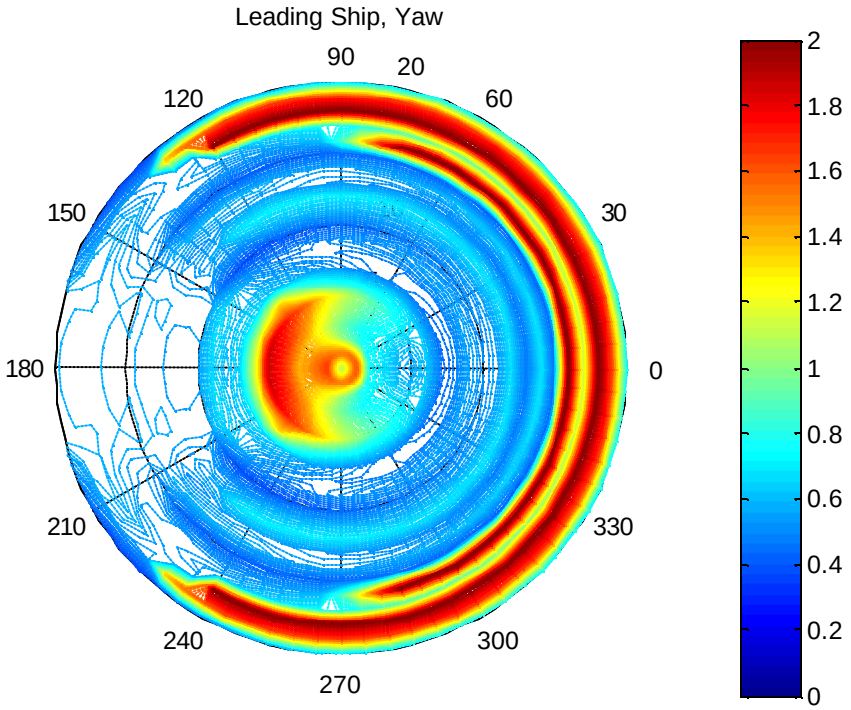

Figure A-9. SLICE Yaw Amplitude Motion (HS: 5 feet, T_m: 5 sec., l/L: 0.1)

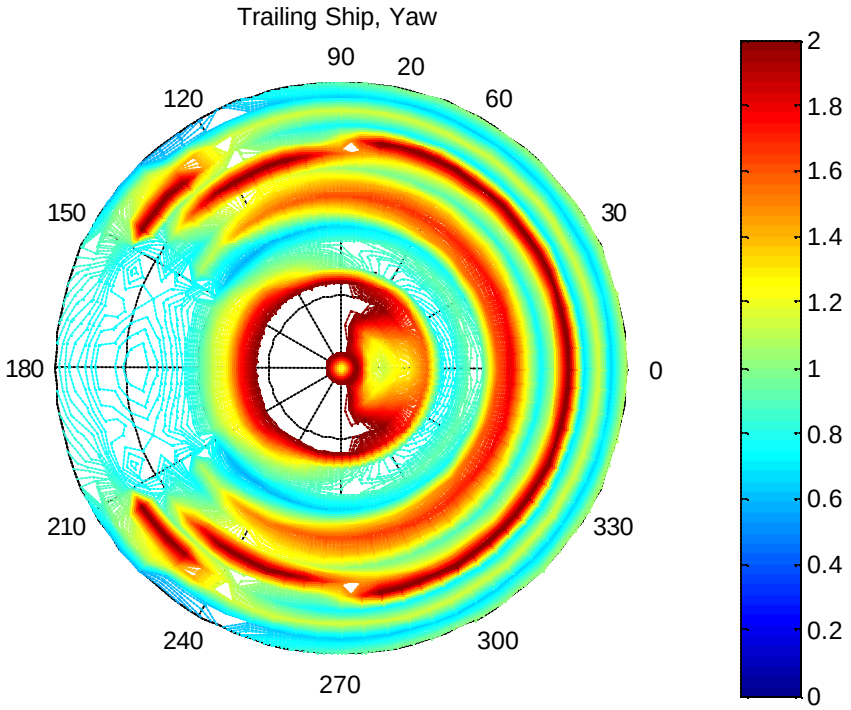

Figure A-10. KAIMALINO Yaw Amplitude Motion (HS: 5 feet, T_m: 5 sec., l/L: 0.1)

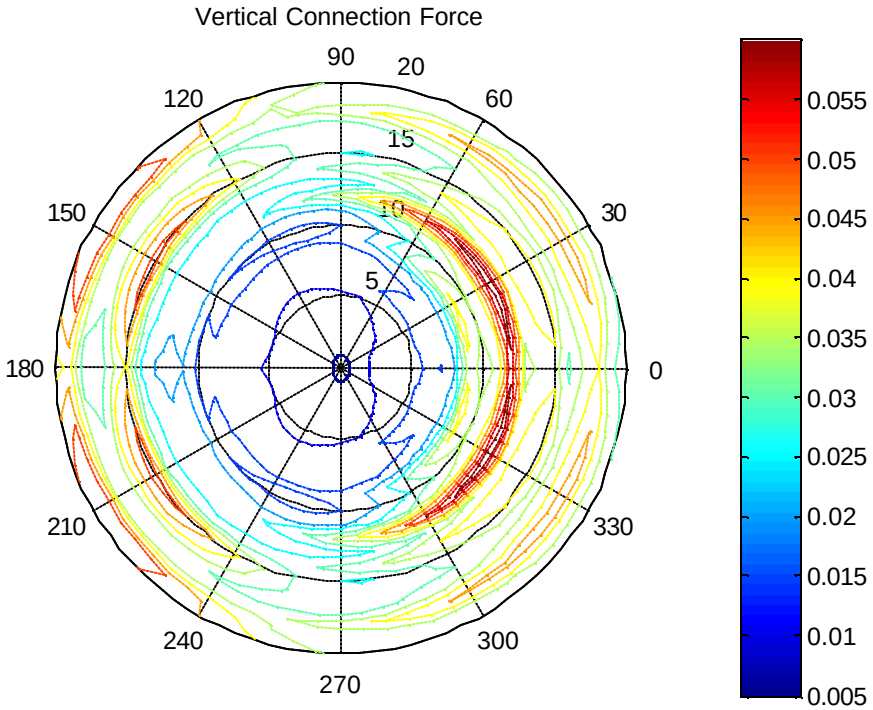

Figure A-351. Vertical Connection Force (HS: 30 feet, T_m: 20 sec., l/L: 1.0)

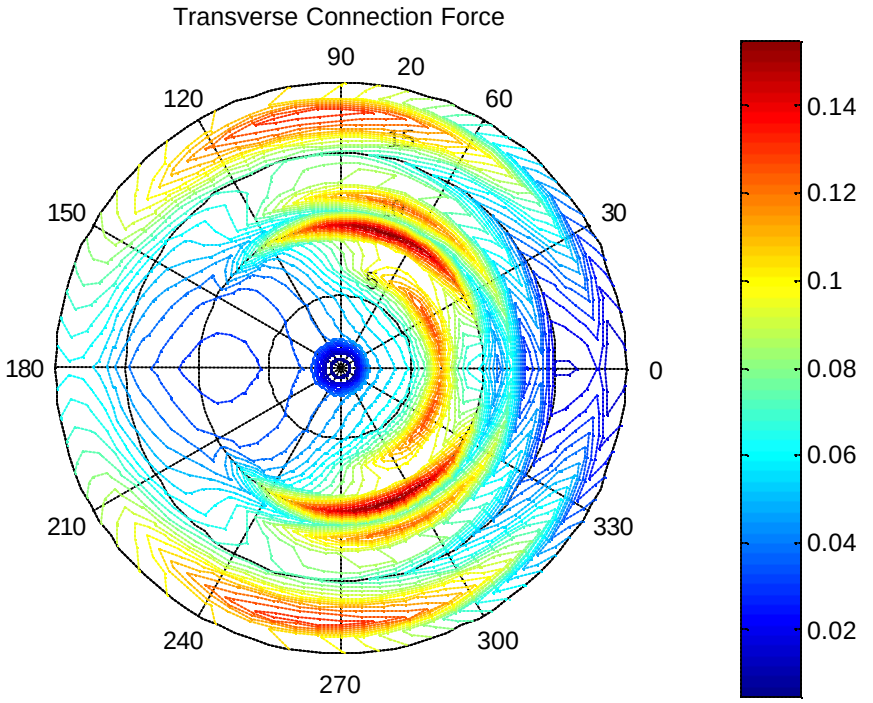

Figure A-352. Transverse Connection Force (HS: 30 feet, T_m: 20 sec., l/L: 1.0)

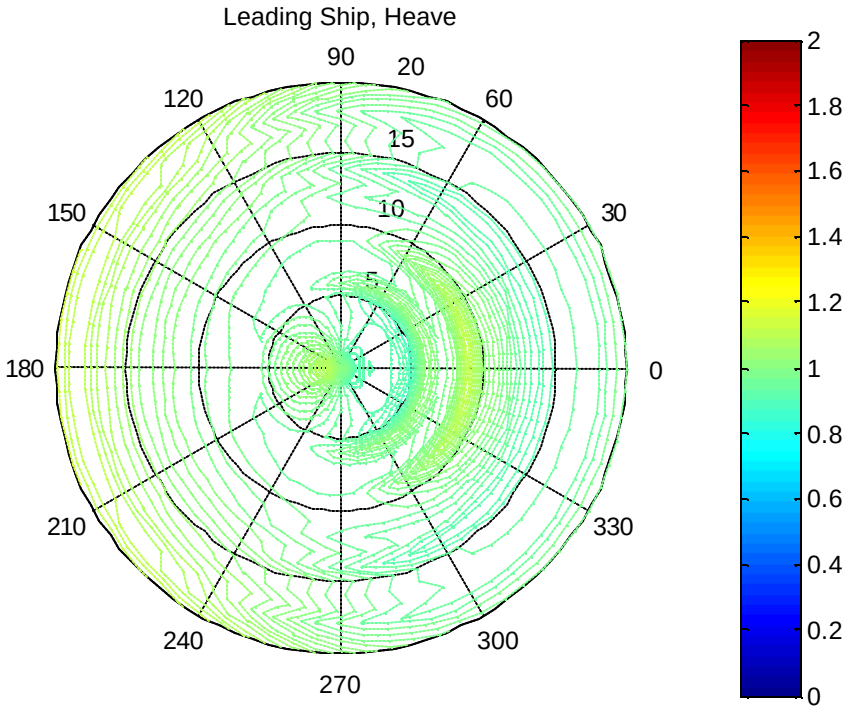

Figure A-353. SLICE Heave Amplitude Motion (HS: 30 feet, T_m: 20 sec., l/L: 1.0)

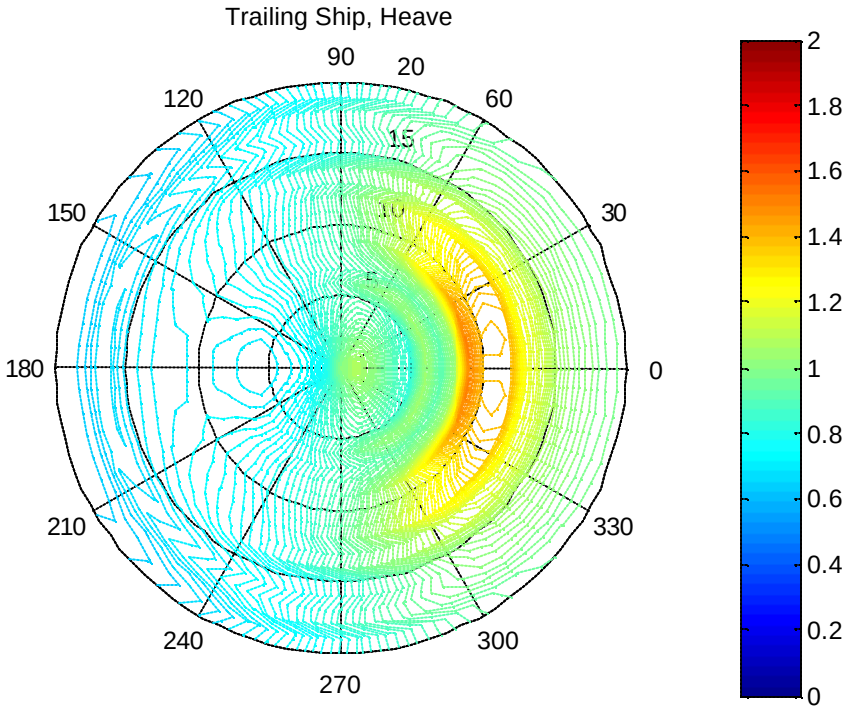

Figure A-354. KAIMALINO Heave Amplitude Motion (HS: 30 feet, T_m: 20 sec., l/L: 1.0)

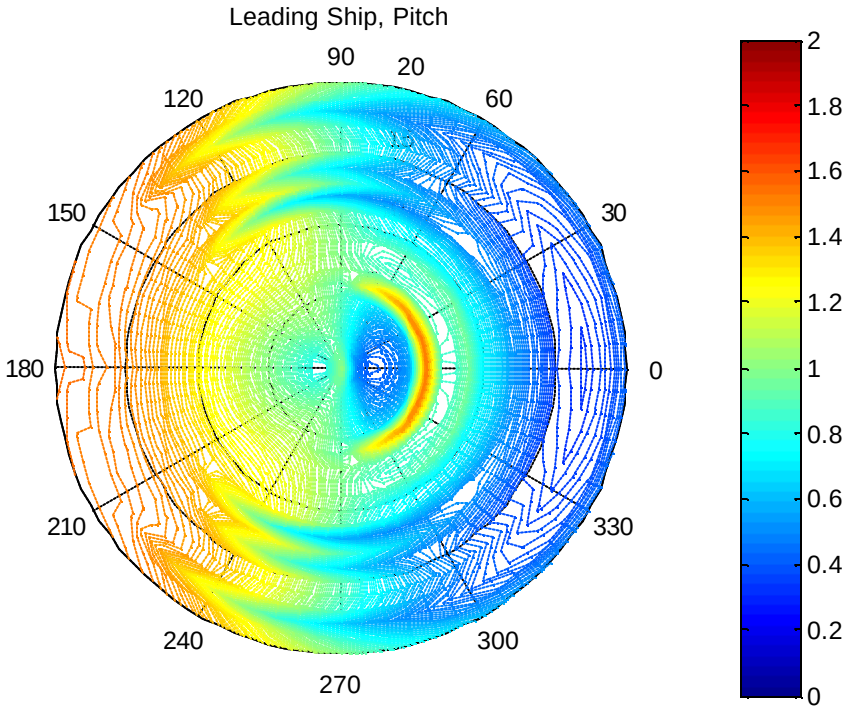

Figure A-355. SLICE Pitch Amplitude Motion (HS: 30 feet, T_m: 20 sec., l/L: 1.0)

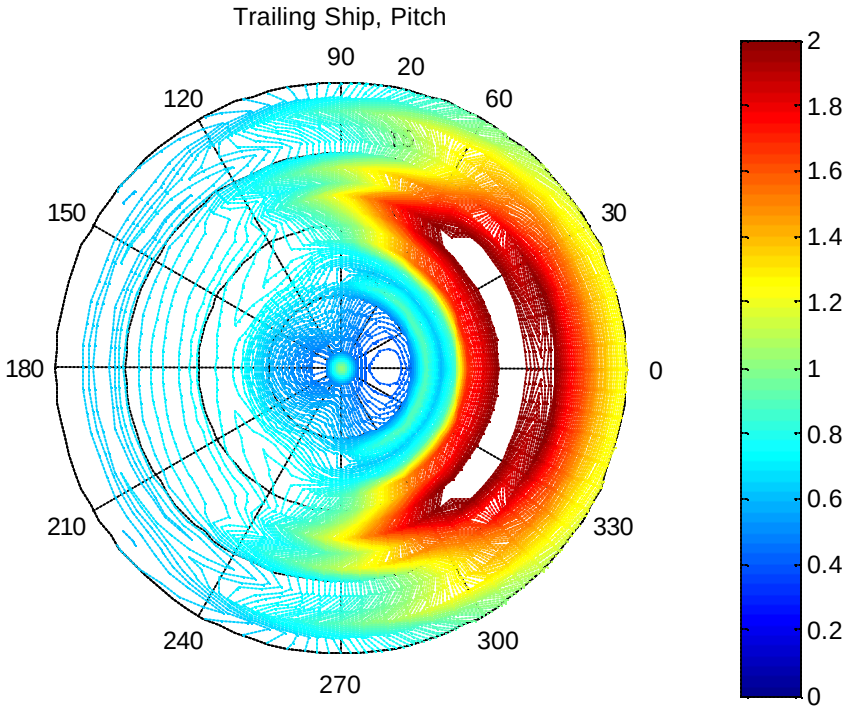

Figure A-356. KAIMALINO Pitch Amplitude Motion (HS: 30 feet, T_m: 20 sec., l/L: 1.0)

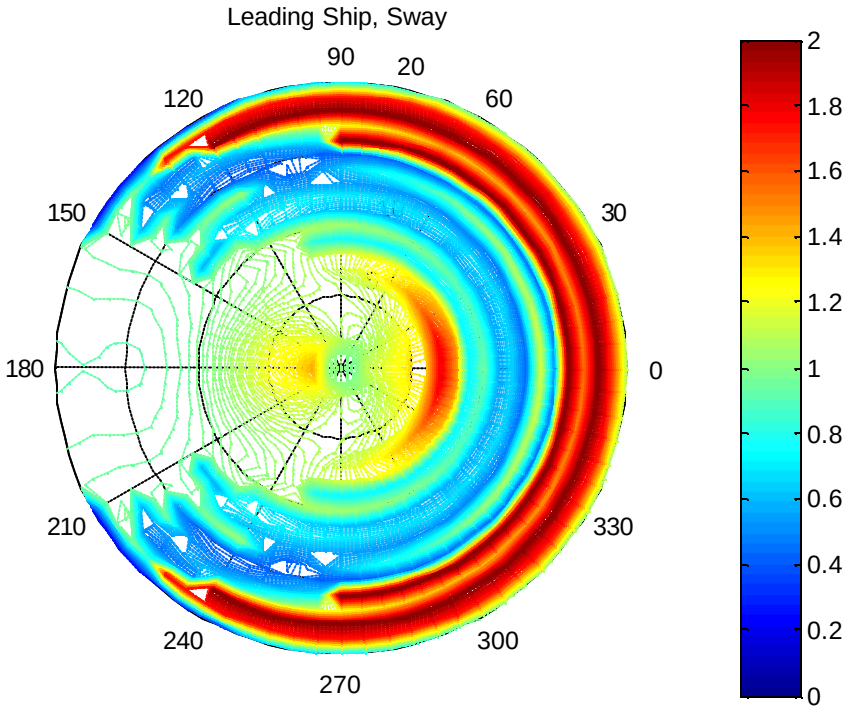

Figure A-357. SLICE Sway Amplitude Motion (HS: 30 feet, T_m: 20 sec., l/L: 1.0)

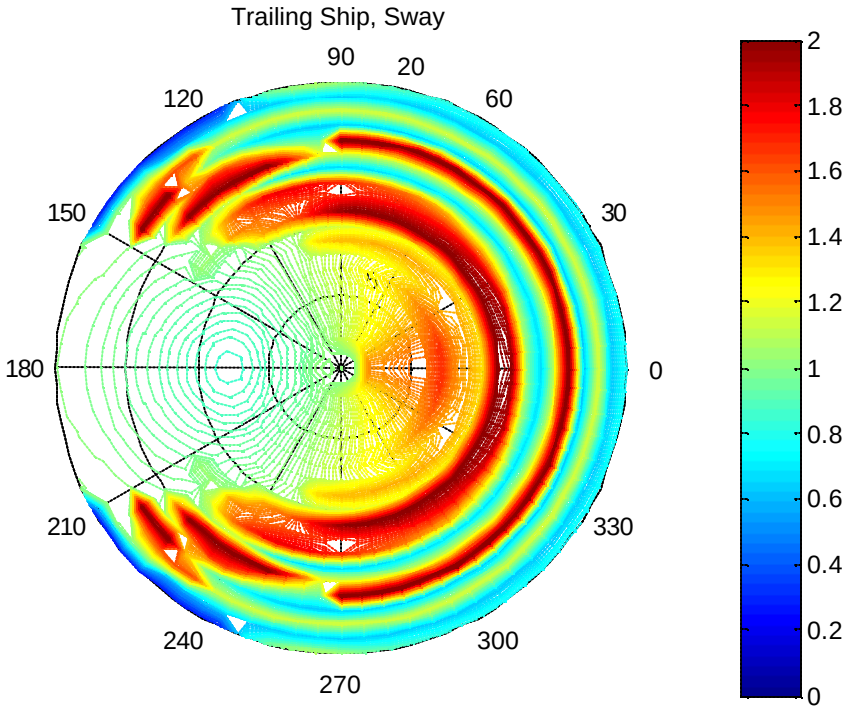

Figure A-358. KAIMALINO Sway Amplitude Motion (HS: 30 feet, T_m: 20 sec., l/L: 1.0)

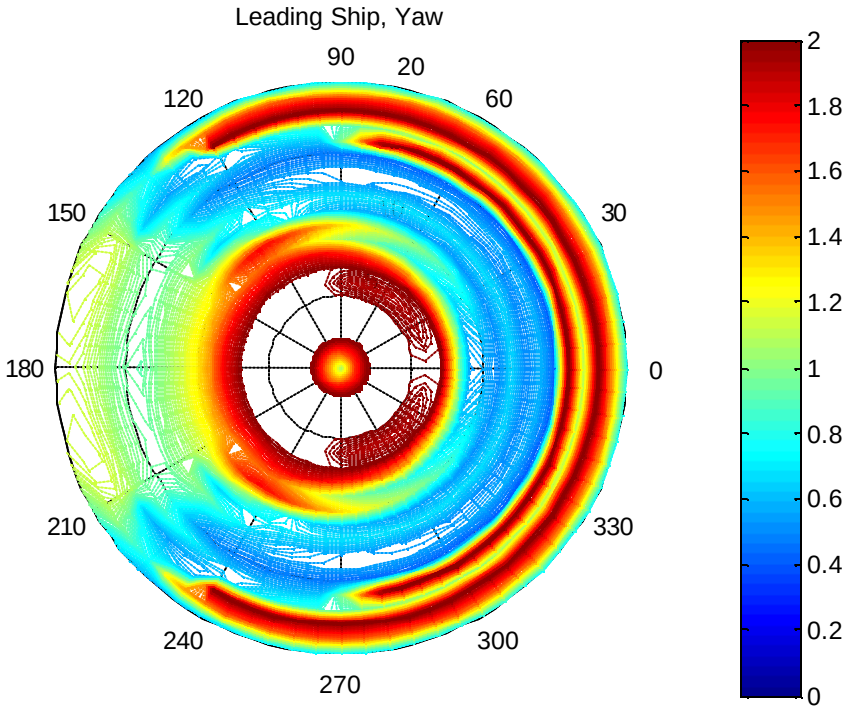

Figure A-359. SLICE Yaw Amplitude Motion (HS: 30 feet, T_m: 20 sec., l/L: 1.0)

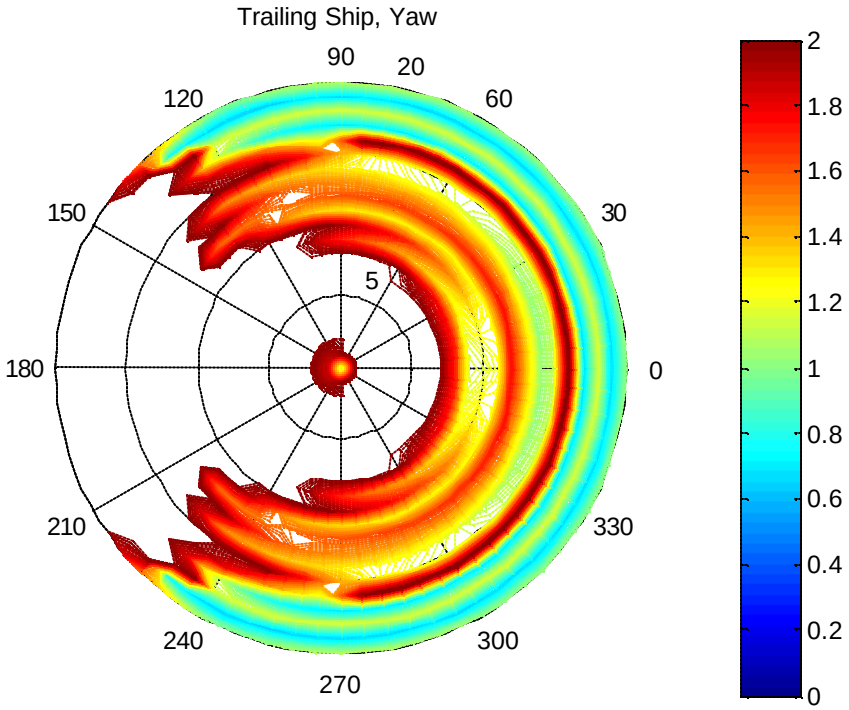

Figure A-360. KAIMALINO Yaw Amplitude Motion (HS: 30 feet, T_m: 20 sec., l/L: 1.0)

THIS PAGE INTENTIONALLY LEFT BLANK

APPENDIX B. FUNDAMENTAL HYDRODYNAMIC THEORY

The six-degree of freedom motion of the SLICE/KAIMALINO vessel configuration in-tow requires a fairly good understanding of the three dimensional motion and the corresponding wave hydrodynamics. In order to investigate the motions on the ocean surface (particularly wave velocity), we must first develop the basic equations (and understanding) of the hydrodynamics of an ideal (nonviscous) fluid. In our study, we assumed that the water is incompressible, the density is constant and the flow is irrotational. These are standard assumptions in seakeeping studies. We also assumed that the ships operate in infinitely deep water. The characterizations are as follows: (1) kinematic equations; (2) conservation of mass (continuity equation); (3) dynamic equations or Bernoulli's equation describing irrotational motion of an incompressible fluid.

Using lagrangian techniques, we can describe any number of particles and their relative positions with respect to the fluid motion. Letting $\mathrm{E} \equiv \mathrm{E}(x, y, z, t)$ stand for a (scalar) property of the ocean wave medium, the lagrangian rate of change for a particle function, E, for some fixed point r_o:

$$\mathrm{E}_o \equiv \mathrm{E}(x_o, y_o, z_o, t_o) \quad (1)$$

When a particle at point r at the time, t, arrives at a neighboring point at the time, t+dt, the function E is the following:

$$\mathrm{E}(x_o + dc, y_o + dy, z_o + dz, t_o + dt) = \mathrm{E}_o + \left(\frac{\partial \mathrm{E}}{\partial x}\right)_o dc + \left(\frac{\partial \mathrm{E}}{\partial y}\right)_o dy + \left(\frac{\partial \mathrm{E}}{\partial z}\right)_o dz + \left(\frac{\partial \mathrm{E}}{\partial t}\right)_o dt \quad (2)$$

Whereby the time rate of change of E from the lagrangian point of view:

$$\frac{d\mathrm{E}}{dt} = n \cdot \nabla \mathrm{E} + \frac{\partial \mathrm{E}}{\partial t} \quad (3)$$

where,

$$n = i\frac{\partial c}{\partial t} + j\frac{\partial y}{\partial t} + k\frac{\partial z}{\partial t}$$
$$\nabla \mathrm{E} = i\frac{\partial \mathrm{E}}{\partial x} + j\frac{\partial \mathrm{E}}{\partial y} + k\frac{\partial \mathrm{E}}{\partial z} \quad (4)$$

Thus is described the general kinematic equation of a water particle.

For our assumptions of an incompressible fluid, which is an accurate model of the ocean medium at the surface where the pressure changes are minimal, the continuity equation resolves to:

$$\nabla \cdot n = 0 \quad (5)$$

where n is the displacement velocity which is derivable from the velocity potential, f, whereby the velocity potential in an incompressible fluid must satisfy Laplace's equation:

$$\nabla \cdot \nabla f = 0 \quad (6)$$

The surface wave is the manifestation of pressure changes and water-particle motions affecting the entire body of fluid- in a column sense all the way through its respective depth, surface to ocean floor. The motion of particles under the idealized given conditions can be characterized by this velocity potential, f. From this function all desired wave properties can be determined.

We shall now derive the Bernoulli Equation by applying Newton's second law to the mass $\rho\Delta\tau$ in an element of volume $\Delta\tau$ of a fluid. The net force acting on the element to give it an acceleration dv/dt includes an external body force, F_e (due to gravity), and an internal force F_i (pressure gradients within the fluid). The pressure force between each element can be described as follows:

$$\Delta F_i = -\nabla P \Delta t \quad (7)$$

$$\Delta F_e = -r\nabla\Omega\Delta t \quad (8)$$

where Ω is the gravitational potential energy per unit mass, $g=-\nabla\Omega$ (i.e. positive y-axis is directed upward, then $\Omega=gy$, and $g=-jg$.

F=ma (9)

$$-\nabla P\Delta t - r\nabla\Omega\Delta t = r\frac{dn}{dt}\Delta t \quad (10)$$

referring to our earlier discussion of equation (3),

$$\frac{d\mathrm{E}}{dt} = n\cdot\nabla\mathrm{E} + \frac{\partial\mathrm{E}}{\partial t} \quad (11)$$

we may now express the acceleration as follows:

$$-\nabla P - r\nabla\Omega = n\cdot\nabla n + \frac{\partial n}{\partial t} \quad (12)$$

When generally discussing waves on the surface of a liquid, it is customary to assume that the liquid particle motion is irrotational. This means that the curl of ν everywhere vanishes, and essentially the mathematical characteristics of eddies, or vorticites is lost and obviously not of our concern. When described in an ideal fluid, these vortices persist forever to conserve angular momentum; however, in reality vortices die out due to fluid viscosity (i.e. smoke rings). Therefore,

$$\nabla\times n = 0 \quad (13)$$

and,

$$(\nabla\times n)\times n = n\cdot\nabla n - \nabla n\cdot n = 0 \quad (14)$$

so that:

$$n\cdot\nabla n = (\nabla n)\cdot n = \nabla\left(\tfrac{1}{2}n^2\right) \quad (15)$$

The no curl condition is a necessary and sufficient condition that ν can be derived from the velocity potential ϕ.

$$n = -\nabla f \quad (16)$$

and since,

$$\frac{\partial n}{\partial t} = -\nabla\frac{\partial f}{\partial t} \quad (17)$$

equation 10 becomes:

$$-\frac{1}{r}\nabla P - \nabla\Omega = -\nabla\frac{\partial f}{\partial t} + \nabla\left(\tfrac{1}{2}n^2\right) \quad (18)$$

integration can then be carried through by dotting dr into it and noting that:

$$d\mathrm{E} = dr \cdot \nabla\mathrm{E} \quad (19)$$

where $d\mathrm{E}$ is the difference between two neighboring points separated by dr. Equation 18 becomes:

$$-\frac{1}{r}dP - d\Omega = -d\frac{\partial f}{\partial t} + d\left(\tfrac{1}{2}n^2\right) \quad (19)$$

and when integrated gives the relation:

$$\int\frac{dP}{r} = \frac{\partial f}{\partial t} - \Omega - \tfrac{1}{2}n^2 \quad (20)$$

and when considered to be incompressible, we resolve to Bernoulli's Equation:

$$\frac{P}{r} + \Omega + \tfrac{1}{2}n^2 = \frac{\partial f}{\partial t} + F(t) \quad (21)$$

whereby the constant of integration, and any time-dependent component has been absorbed into the undetermined $\frac{\partial f}{\partial t}$ component. Taking the time derivative and treating P as a constant and considering:

$$\begin{aligned} n_x &= \frac{\partial c}{\partial t} = -\frac{\partial f}{\partial x} \\ n_{yx} &= \frac{\partial y}{\partial t} = -\frac{\partial f}{\partial y} \\ n_z &= \frac{\partial z}{\partial t} = -\frac{\partial f}{\partial z} \end{aligned} \quad (22)$$

evaluating y=h, we find:

$$n_y = -\frac{\partial f}{\partial y} = \frac{1}{g}\frac{\partial^2 f}{dt^2} \quad (23)$$

showing that velocity depends on position and time, Bernoulli's equation can now be used to compute pressure at any point in the fluid. Solving for the velocity potential

function and knowing that it is a function of position and time, we must satisfy the Laplace equation:

$$\frac{\partial^2 f}{dx^2} + \frac{\partial^2 f}{dy^2} = 0 \quad (24)$$

where;

$$f(x, y, t) = X(x) \cdot Y(t) \cdot T(t) \quad (25)$$

The spatial functions are determined from separation of variables, and the general solution:

$$\begin{aligned} X(x) &= Ae^{ikx} + Be^{-ikx} \\ Y(y) &= Ce^{ky} + De^{-ky} \end{aligned} \quad (26)$$

considering the boundary conditions at y=0:

$$n_y = -\frac{\partial f}{\partial y} = -XT\frac{dY}{dy} = 0 \quad (27)$$

which requires that C=D, where;

$$Y(y) = 2C\cosh(ky) \quad (28)$$

similarly the velocity potential has the form:

$$f = A\cosh kye^{ikx}T(t) \quad (29)$$

and substituting into equation 24, we obtain the equation for T(t):

$$\frac{d^2T}{dt^2} + (gk\tanh kh)T = 0 \quad (30)$$

which leads to the simple solution of harmonic time dependence with the angular frequency:

$$w = (gk\tanh kh)^{1/2} \quad (31)$$

wave velocity is then:

$$c = \frac{w}{k} = \left(\frac{g}{k} \tanh\ kh \right)^{1/2} \quad (32)$$

for the case of deep water, say when $h \geq \lambda/2$, $\tanh \kappa h \geq \tanh \pi = 0.996$, so that the expression for the wave velocity becomes rather closely:

$$c = \left(\frac{g}{k} \right)^{1/2} = \left(\frac{lg}{2p} \right)^{1/2}, (\lambda < h) \quad (33)$$

APPENDIX C. VERTICAL PLANE COUPLING DERIVATION

Defining the equations of motions for a point on the each of the SLICE and the KAIMALINO:

$$[\Delta_S + A_S]\{\ddot{h}\} + [B_S]\{\dot{h}\} + [C_S]\{h\} = \{F_{ex}\} + \{f_S\} \quad (1)$$

$$[\Delta_K + A_K]\{\ddot{h}\} + [B_K]\{\dot{h}\} + [C_K]\{h\} = \{F_{ex}\} + \{f_K\} \quad (2)$$

where f_S and f_K are the connection forces acting on SLICE and KAIMALINO respectively, where $f_K = -f_S$. The connection forces and absolute motions are illustrated in Figure C 1.

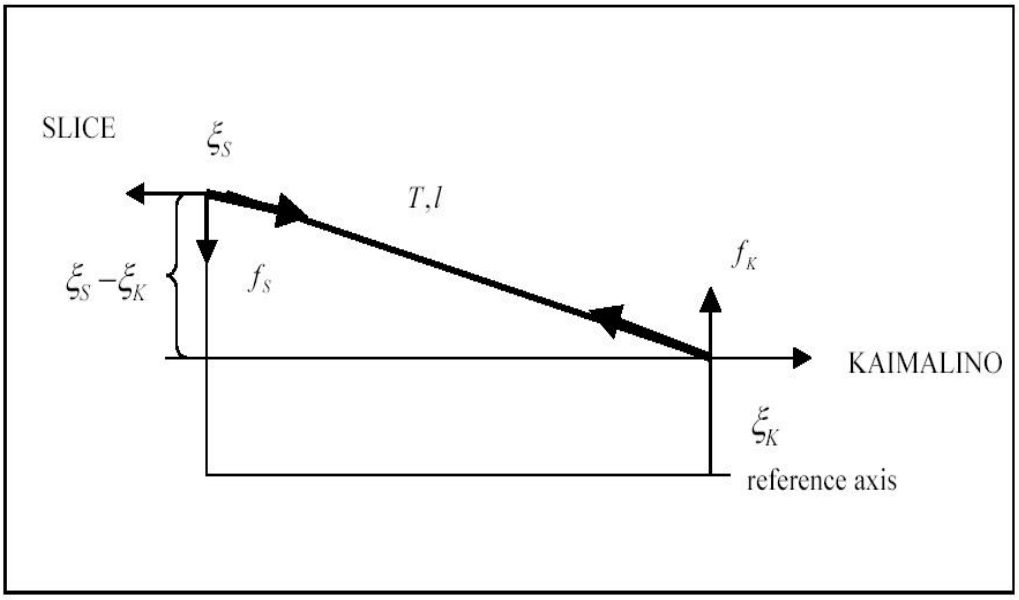

Figure C 1. Connection Force and Motions of the Ships (From: Orhan)

Continuing with the derivation of Equation (39):

$$[-w_e{}^2(\Delta + A) + iw_e B + C]\{\bar{h}\} = \{F_{ex}\} + \{f\} \quad (3)$$

Since the exponential exists in all terms, it is canceled and the equations of motion in the frequency domain become as follows:

$$\bar{A} = [-w_e{}^2(\Delta + A) + iw_e B + C] \quad (4)$$

We know that $\overline{A}$ is a 6x6 matrix for six degrees of freedom system:

$$\overline{A}\overline{h} = \{F\} \quad (5)$$

$$\overline{h} = inv(\overline{A})\{F\} \quad (6)$$

where;

$$\{F\} = \{F_{ex}\} + \{f\} \quad (7)$$

Ship motions due to regular waves of a given wavelength and direction are now determined for a given forward speed (V). Motions in vertical and horizontal planes are decoupled for our discussion and may be solved as two distinct 3x3 systems. The heave and pitch modes and the resultant interactions will be derived from this point forward (sway and yaw are similar). The expanded equations of motion in two degrees of freedom become as:

$$\begin{bmatrix} \overline{A}_{33} & \overline{A}_{35} \\ \overline{A}_{53} & \overline{A}_{55} \end{bmatrix} \begin{bmatrix} h_3 \\ h_5 \end{bmatrix} = \begin{bmatrix} F_3 + f \\ F_5 + fx_s \end{bmatrix} \quad (11)$$

Now we can define the equations of motion in vertical plane (two degrees of freedom) for the two vessels as:

$$\overline{A}_{33,s}\overline{h}_{3,S} + \overline{A}_{35,S}\overline{h}_{5,S} = F_{3,S} + f_S \quad (12)$$

$$\overline{A}_{53,s}\overline{h}_{3,S} + \overline{A}_{55,S}\overline{h}_{5,S} = F_{5,S} - f_S x_S \quad (13)$$

$$\overline{A}_{33,K}\overline{h}_{3,K} + \overline{A}_{35,K}\overline{h}_{5,K} = F_{3,K} + f_K \quad (14)$$

$$\overline{A}_{53,K}\overline{h}_{3,K} + \overline{A}_{55,K}\overline{h}_{5,K} = F_{5,K} - f_S x_K \quad (15)$$

where x is the distance between the connection point and the center of gravity of that vehicle. In order to solve these four equations, we make the following substitution:

$$\begin{aligned}
\bar{h}_{3,S} &= m_{3,S} + n_{3,S} f_S \\
\bar{h}_{5,S} &= m_{5,S} + n_{5,S} f_S \\
\bar{h}_{3,K} &= m_{3,K} + n_{3,K} f_K \\
\bar{h}_{5,K} &= m_{5,K} + n_{5,K} f_K
\end{aligned} \quad (16)$$

where;

$$f_S = -f_K = -f \quad (17)$$

Using Cramer's Rule, the absolute motions can be described by (Nash):

$$\begin{aligned}
x_S &= \bar{h}_{3,S} - \bar{h}_{5,S} x_S \\
x_K &= \bar{h}_{3,K} - \bar{h}_{5,K} x_K
\end{aligned} \quad (18)$$

When we combine (13) and (14) as:

$$\begin{aligned}
x_S &= m_{3,S} - n_{3,S} f - m_{5,S} x_S + n_{5,S} x_S f \\
x_K &= m_{3,K} + n_{3,K} f - m_{5,K} x_K - n_{5,K} x_K f
\end{aligned} \quad (19)$$

Let a in terms of m's and b in terms of n's be defined as:

$$\begin{aligned}
a &= m_{3,S} - m_{3,K} + m_{5,K} x_K - m_{5,S} x_S \\
b &= -n_{3,S} - n_{3,K} + n_{5,K} x_K + n_{5,S} x_S
\end{aligned} \quad (20)$$

Therefore, our equation of motion becomes:

$$x_S - x_K = a - bf \quad (21)$$

Again referring to Figure 2,

$$f = T \frac{x_S - x_K}{l} \quad (22)$$

Combining (17) and (18) gives us our final equation, which gives us the connection force between two ships:

$$f = \frac{a}{\frac{l}{T} + b} \quad (23)$$

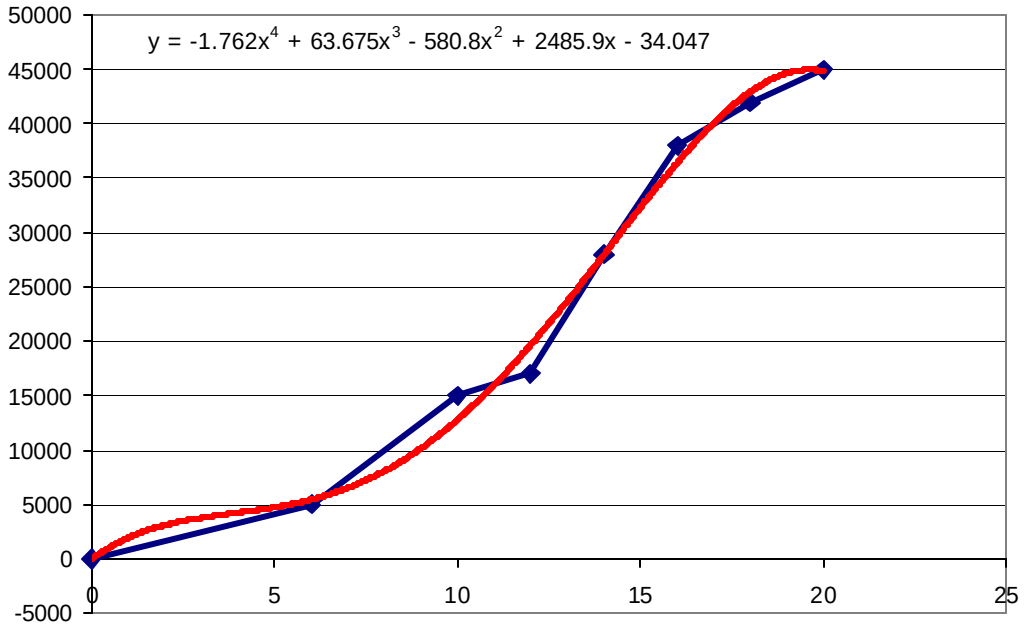

Figure C 2. KAIMALINO Tension vs. Speed Plot (After: Lockheed Martin)

APPENDIX D. MATLAB COUPLING ALGORITHM

```
% Horizontal Plane
% Dimensional version (U.S. units)
% Contour plots (heading/speed)
% Two parameter Bretschneider spectrum - Short crested seas

%
% Get run info
%
HS=input('Significant Wave Height (feet) = ');
T_m=input('Modal Period (sec) = ');
l=input('Length (l/L)  = ');
%
omega_m=2*pi/T_m;
HS_string=num2str(HS);
warning off
%
lambda_min=20;                  % Min wave length (ft)
lambda_max=1000;                % Max wave length (ft)
delta_lambda=20;                % Wave length increment (ft)
rho=1.9905;                     % Water density
zeta=1;                         % Regular wave height
L=105;                          % Reference length for nondimensionalization
g=32.2;                         % Gravitational constant
x_s=-46;                        % FRONT SHIP attachment point
x_k=+40;                        % REAR SHIP attachment point
beta_incr=5;                    % Increment in sea direction (deg)
motion_ratio=2;                 % Ratio for motion plotting comparison
%
% The matdata output files default to the vertical only format when the
% heading angle is 0 or 180 degrees.
% Set up file reading format.
%
%
% GENERAL DATA
%
lambda=lambda_min:delta_lambda:lambda_max;          % Vector of wavelengths
wavenumber=2.0*pi./lambda;                          % Wave number
omega=sqrt(wavenumber*g);                           %Wave frequency
period=2.0*pi./omega;
omega=omega';
filesize=size(lambda);
if beta_incr==15
   load data_15;             % Load main data file, 15 deg. heading increments
   beta_incr_values=13;
end
if beta_incr==5
   load data_5;              % Load main data file, 5 deg. heading increments
   beta_incr_values=37;
end
%
```

```
% Random wave calculations
% Bretschneider spectrum - weighted by the spreading function
%
iSpeed=0;
for V_knots=0:1:20,       % Loop on speed
   iSpeed=iSpeed+1;
   %
   % Get tension from curvefitting data.
   % Applicable for speeds between 1 and 20 ft/sec.
   %
   T=-1.762*V_knots^4+63.675*V_knots^3-580.8*V_knots^2+2485.9*V_knots-34.047;
   %
   V_string=num2str(V_knots)
   V=V_knots*1.6878;                    % Convert to ft/sec
   A=(1.25/4)*(omega_m^4)*(HS^2);
   B=1.25*omega_m^4;
   S_main=(A./omega.^5).*exp(-B./omega.^4);
   %
   ibeta=0;
   for beta=0:beta_incr:360,            % Loop on sea direction
      beta_set=beta;
      if beta>180
         beta_set=360-beta;
      end
      ibeta=ibeta+1;
      beta;
      %
      % Spreading between (beta-90) and (beta+90)
      %
      beta_spread_low =beta_set - 90;
      beta_spread_high=beta_set + 90;
      ibeta_spread=0;
      %
      % Loop between (beta-90) and (beta+90)
      % Use either 15 deg increments (13 values total) or
      % 5 deg increments (total of 37 values)
      %
      for beta_spread=beta_spread_low:beta_incr:beta_spread_high,
         ibeta_spread=ibeta_spread + 1;
         beta_spread_read=beta_spread;
         beta_spread_vector(ibeta_spread)=beta_spread;
         if beta_spread<0
            beta_spread_read=-beta_spread;
         end
         if beta_spread>180
            beta_spread_read=360-beta_spread;
         end
         beta_string=num2str(beta_spread_read);
         trigg=30;
         f2loc=26; f6loc=30;
         if beta_spread_read==0
            trigg=27;
         f2loc=25; f6loc=27;
```

```
elseif beta_spread_read==180
   trigg=27;
   f2loc=25; f6loc=27;
end
lambda_size=trigg*filesize(2);
%
% Load FRONT SHIP data file msvhV_beta.txt
%
load_filename=strcat('msvh',V_string,'_',beta_string);
filename_s=eval(load_filename);
%
% Load REAR SHIP data file
%
load_filename=strcat('mkvh',V_string,'_',beta_string);
filename_k=eval(load_filename);
omegae=omega'-wavenumber*V*cos(beta_spread*pi/180); %Freq. of Encounter
omegae=omegae';
periode=2.0*pi./omegae;
%
% HORIZONTAL PLANE RESPONSE CALCULATIONS
%
% SLICE
%
% Set mass matrix elements
%
M22s=filename_s(2:trigg:lambda_size,2);
M26s=filename_s(2:trigg:lambda_size,6);
M62s=filename_s(6:trigg:lambda_size,2);
M66s=filename_s(6:trigg:lambda_size,6);
%
% Added mass terms
%
A22s=filename_s(8:trigg:lambda_size,2);
A26s=filename_s(8:trigg:lambda_size,6);
A62s=filename_s(12:trigg:lambda_size,2);
A66s=filename_s(12:trigg:lambda_size,6);
%
% Damping terms
%
B22s=filename_s(14:trigg:lambda_size,2);
B26s=filename_s(14:trigg:lambda_size,6);
B62s=filename_s(18:trigg:lambda_size,2);
B66s=filename_s(18:trigg:lambda_size,6);
%
% Hydrostatic terms
%
C22s=filename_s(20:trigg:lambda_size,2);
C26s=filename_s(20:trigg:lambda_size,6);
C62s=filename_s(24:trigg:lambda_size,2);
C66s=filename_s(24:trigg:lambda_size,6);
%
if beta_spread==0
   F2s_t=zeros(50,1); F6s_t=zeros(50,1);
```

```
elseif beta_spread==180
   F2s_t=zeros(50,1); F6s_t=zeros(50,1);
else
   %
   % Total exciting forces
   %
   F2s_t_amp=filename_s(f2loc:trigg:lambda_size,5);
   F6s_t_amp=filename_s(f6loc:trigg:lambda_size,5);
   F2s_t_pha=filename_s(f2loc:trigg:lambda_size,6);
   F6s_t_pha=filename_s(f6loc:trigg:lambda_size,6);
   F2s_t=F2s_t_amp.*exp(i*F2s_t_pha.*pi/180.0);
   F6s_t=F6s_t_amp.*exp(i*F6s_t_pha.*pi/180.0);
   %
   % Froude/Krylov exciting forces
   %
   F2s_f_amp=filename_s(f2loc:trigg:lambda_size,1);
   F6s_f_amp=filename_s(f6loc:trigg:lambda_size,1);
   F2s_f_pha=filename_s(f2loc:trigg:lambda_size,2);
   F6s_f_pha=filename_s(f6loc:trigg:lambda_size,2);
   F2s_f=F2s_f_amp.*exp(i*F2s_f_pha.*pi/180.0);
   F6s_f=F6s_f_amp.*exp(i*F6s_f_pha.*pi/180.0);
   %
   % Diffraction exciting forces
   %
   F2s_d_amp=filename_s(f2loc:trigg:lambda_size,3);
   F6s_d_amp=filename_s(f6loc:trigg:lambda_size,3);
   F2s_d_pha=filename_s(f2loc:trigg:lambda_size,4);
   F6s_d_pha=filename_s(f6loc:trigg:lambda_size,4);
   F2s_d=F2s_d_amp.*exp(i*F2s_d_pha.*pi/180.0);
   F6s_d=F6s_d_amp.*exp(i*F6s_d_pha.*pi/180.0);
   %
end
% KAIMALINO
%
% Set mass matrix elements
%
M22k=filename_k(2:trigg:lambda_size,2);
M26k=filename_k(2:trigg:lambda_size,6);
M62k=filename_k(6:trigg:lambda_size,2);
M66k=filename_k(6:trigg:lambda_size,6);
%
% Added mass terms
%
A22k=filename_k(8:trigg:lambda_size,2);
A26k=filename_k(8:trigg:lambda_size,6);
A62k=filename_k(12:trigg:lambda_size,2);
A66k=filename_k(12:trigg:lambda_size,6);
%
% Damping terms
%
B22k=filename_k(14:trigg:lambda_size,2);
B26k=filename_k(14:trigg:lambda_size,6);
B62k=filename_k(18:trigg:lambda_size,2);
```

```
B66k=filename_k(18:trigg:lambda_size,6);
%
% Hydrostatic terms
%
C22k=filename_k(20:trigg:lambda_size,2);
C26k=filename_k(20:trigg:lambda_size,6);
C62k=filename_k(24:trigg:lambda_size,2);
C66k=filename_k(24:trigg:lambda_size,6);
if beta_spread==0
   F2k_t=zeros(50,1); F6k_t=zeros(50,1);
elseif beta_spread==180
   F2k_t=zeros(50,1); F6k_t=zeros(50,1);
else
   %
   % Total exciting forces
   %
   F2k_t_amp=filename_k(f2loc:trigg:lambda_size,5);
   F6k_t_amp=filename_k(f6loc:trigg:lambda_size,5);
   F2k_t_pha=filename_k(f2loc:trigg:lambda_size,6);
   F6k_t_pha=filename_k(f6loc:trigg:lambda_size,6);
   F2k_t=F2k_t_amp.*exp(i*F2k_t_pha.*pi/180.0);
   F6k_t=F6k_t_amp.*exp(i*F6k_t_pha.*pi/180.0);
   %
   % Froude/Krylov exciting forces
   %
   F2k_f_amp=filename_k(f2loc:trigg:lambda_size,1);
   F6k_f_amp=filename_k(f6loc:trigg:lambda_size,1);
   F2k_f_pha=filename_k(f2loc:trigg:lambda_size,2);
   F6k_f_pha=filename_k(f6loc:trigg:lambda_size,2);
   F2k_f=F2k_f_amp.*exp(i*F2k_f_pha.*pi/180.0);
   F6k_f=F6k_f_amp.*exp(i*F6k_f_pha.*pi/180.0);
   %
   % Diffraction exciting forces
   %
   F2k_d_amp=filename_k(f2loc:trigg:lambda_size,3);
   F6k_d_amp=filename_k(f6loc:trigg:lambda_size,3);
   F2k_d_pha=filename_k(f2loc:trigg:lambda_size,4);
   F6k_d_pha=filename_k(f6loc:trigg:lambda_size,4);
   F2k_d=F2k_d_amp.*exp(i*F2k_d_pha.*pi/180.0);
   F6k_d=F6k_d_amp.*exp(i*F6k_d_pha.*pi/180.0);
end
%
% MATCHING CONDITION
%
A22bar_s=-(omegae.^2).*(M22s+A22s)+i*omegae.*B22s+C22s;
A26bar_s=-(omegae.^2).*(M26s+A26s)+i*omegae.*B26s+C26s;
A62bar_s=-(omegae.^2).*(M62s+A62s)+i*omegae.*B62s+C62s;
A66bar_s=-(omegae.^2).*(M66s+A66s)+i*omegae.*B66s+C66s;
A22bar_k=-(omegae.^2).*(M22k+A22k)+i*omegae.*B22k+C22k;
A26bar_k=-(omegae.^2).*(M26k+A26k)+i*omegae.*B26k+C26k;
A62bar_k=-(omegae.^2).*(M62k+A62k)+i*omegae.*B62k+C62k;
A66bar_k=-(omegae.^2).*(M66k+A66k)+i*omegae.*B66k+C66k;
%
```

```
   A26_s_den=(A22bar_s.*A66bar_s-A26bar_s.*A62bar_s);
   A26_k_den=(A22bar_k.*A66bar_k-A62bar_k.*A26bar_k);
   %
   mu2_s=(A66bar_s.*F2s_t-A26bar_s.*F6s_t)./A26_s_den;
   nu2_s=(A66bar_s-A26bar_s*x_s)./A26_s_den;
   mu6_s=(A22bar_s.*F6s_t-A62bar_s.*F2s_t)./A26_s_den;
   nu6_s=(A22bar_s*x_s-A62bar_s)./A26_s_den;
   mu2_k=(A66bar_k.*F2k_t-A26bar_k.*F6k_t)./A26_k_den;
   nu2_k=(A66bar_k-A26bar_k*x_k)./A26_k_den;
   mu6_k=(A22bar_k.*F6k_t-A62bar_k.*F2k_t)./A26_k_den;
   nu6_k=(A22bar_k*x_k-A62bar_k)./A26_k_den;
   %
   a=mu2_s+mu6_s*x_s-mu2_k-mu6_k*x_k;
   b=nu2_s+nu6_s*x_s+nu2_k+nu6_k*x_k;
   f=a./(l/T+b);
   %
   f_s=-f;                                % Connection force on SLICE
   f_k=f;                                 % Connection force on KAIMALINO
   eta2_s=mu2_s+nu2_s.*f_s;               % SLICE sway
   eta6_s=mu6_s+nu6_s.*f_s;               % SLICE yaw
   eta2_k=mu2_k+nu2_k.*f_k;               % KAIMALINO sway
   eta6_k=mu6_k+nu6_k.*f_k;               % KAIMALINO yaw
   xi_s=eta2_s+eta6_s*x_s;                % SLICE motion at connection
   xi_k=eta2_k+eta6_k*x_k;                % KAIMALINO motion at connection
   xi0_s=mu2_s+mu6_s*x_s;                 % SLICE motion at connection for zero f
   xi0_k=mu6_k+mu6_k*x_k;                 % KAIMALINO motion at connection for zero f
   delta_beta(ibeta_spread)=beta_set-beta_spread;
   S=S_main *(2/pi)*(cos((beta_set-beta_spread)*pi/180))^2;      % Mult.by (2/pi)cos^2
   Se=S./abs((1-(2.0/g)*omega*V*cos(beta_spread*pi/180)));      % S(w) to S(we)
   %
   % Define response spectra and store as functions of theta
   %
   Sf(:,ibeta_spread)=((abs(f)).^2).*Se;
   Sxi_s(:,ibeta_spread)=((abs(xi_s)).^2).*Se;
   Sxi_k(:,ibeta_spread)=((abs(xi_k)).^2).*Se;
   Sxi0_s(:,ibeta_spread)=((abs(xi0_s)).^2).*Se;
   Sxi0_k(:,ibeta_spread)=((abs(xi0_k)).^2).*Se;
   SF2s_t(:,ibeta_spread)=((abs(F2s_t)).^2).*Se;
   SF2k_t(:,ibeta_spread)=((abs(F2k_t)).^2).*Se;
   Seta2_s(:,ibeta_spread)=((abs(eta2_s)).^2).*Se;
   Smu2_s(:,ibeta_spread)=((abs(mu2_s)).^2).*Se;
   Seta6_s(:,ibeta_spread)=((abs(eta6_s)).^2).*Se;
   Smu6_s(:,ibeta_spread)=((abs(mu6_s)).^2).*Se;
   Seta2_k(:,ibeta_spread)=((abs(eta2_k)).^2).*Se;
   Smu2_k(:,ibeta_spread)=((abs(mu2_k)).^2).*Se;
   Seta6_k(:,ibeta_spread)=((abs(eta6_k)).^2).*Se;
   Smu6_k(:,ibeta_spread)=((abs(mu6_k)).^2).*Se;
end                                       % Loop on beta_spreading ends
%
% Initialize variables before integrating
%
Sf_i=0;
Sxi_s_i=0;
```

```
Sxi_k_i=0;
Sxi0_s_i=0;
Sxi0_k_i=0;
SF2s_t_i=0;
SF2k_t_i=0;
Seta2_s_i=0;
Smu2_s_i=0;
Seta6_s_i=0;
Smu6_s_i=0;
Seta2_k_i=0;
Smu2_k_i=0;
Seta6_k_i=0;
Smu6_k_i=0;
%
% Integrate response spectra over omega and theta
%
for J=2:1:beta_incr_values,   % 13 for 15 deg increments, 37 for 5 deg increments
   for I=2:1:filesize(2),
      %
      delta_omega=abs(omegae(I-1)-omegae(I));
      delta_theta=beta_incr*pi/180;
      %
      Sf_sum=Sf(I,J)+Sf(I-1,J)+Sf(I,J-1)+Sf(I-1,J-1);
      Sxi_s_sum=Sxi_s(I,J)+Sxi_s(I-1,J)+Sxi_s(I,J-1)+Sxi_s(I-1,J-1);
      Sxi_k_sum=Sxi_k(I,J)+Sxi_k(I-1,J)+Sxi_k(I,J-1)+Sxi_k(I-1,J-1);
      Sxi0_s_sum=Sxi0_s(I,J)+Sxi0_s(I-1,J)+ Sxi0_s(I,J-1)  + Sxi0_s(I-1,J-1);
      Sxi0_k_sum=Sxi0_k(I,J)  + Sxi0_k(I-1,J)  + Sxi0_k(I,J-1)  + Sxi0_k(I-1,J-1);
      SF2s_t_sum=SF2s_t(I,J)  + SF2s_t(I-1,J)  + SF2s_t(I,J-1)  + SF2s_t(I-1,J-1);
      SF2k_t_sum=SF2k_t(I,J)  + SF2k_t(I-1,J)  + SF2k_t(I,J-1)  + SF2k_t(I-1,J-1);
      Seta2_s_sum=Seta2_s(I,J) + Seta2_s(I-1,J) + Seta2_s(I,J-1) + Seta2_s(I-1,J-1);
      Smu2_s_sum=Smu2_s(I,J)  + Smu2_s(I-1,J)  + Smu2_s(I,J-1)  + Smu2_s(I-1,J-1);
      Seta6_s_sum=Seta6_s(I,J) + Seta6_s(I-1,J) + Seta6_s(I,J-1) + Seta6_s(I-1,J-1);
      Smu6_s_sum=Smu6_s(I,J)  + Smu6_s(I-1,J)  + Smu6_s(I,J-1)  + Smu6_s(I-1,J-1);
      Seta2_k_sum=Seta2_k(I,J) + Seta2_k(I-1,J) + Seta2_k(I,J-1) + Seta2_k(I-1,J-1);
      Smu2_k_sum=Smu2_k(I,J)  + Smu2_k(I-1,J)  + Smu2_k(I,J-1)  + Smu2_k(I-1,J-1);
      Seta6_k_sum=Seta6_k(I,J) + Seta6_k(I-1,J) + Seta6_k(I,J-1) + Seta6_k(I-1,J-1);
      Smu6_k_sum=Smu6_k(I,J)  + Smu6_k(I-1,J)  + Smu6_k(I,J-1)  + Smu6_k(I-1,J-1);
      %
      Sf_i=Sf_i     + 0.25*delta_omega*delta_theta*Sf_sum;
      Sxi_s_i=Sxi_s_i   + 0.25*delta_omega*delta_theta*Sxi_s_sum;
      Sxi_k_i=Sxi_k_i   + 0.25*delta_omega*delta_theta*Sxi_k_sum;
      Sxi0_s_i=Sxi0_s_i  + 0.25*delta_omega*delta_theta*Sxi0_s_sum;
      Sxi0_k_i=Sxi0_k_i  + 0.25*delta_omega*delta_theta*Sxi0_k_sum;
      SF2s_t_i=SF2s_t_i  + 0.25*delta_omega*delta_theta*SF2s_t_sum;
      SF2k_t_i=SF2k_t_i  + 0.25*delta_omega*delta_theta*SF2k_t_sum;
      Seta2_s_i=Seta2_s_i + 0.25*delta_omega*delta_theta*Seta2_s_sum;
      Smu2_s_i=Smu2_s_i  + 0.25*delta_omega*delta_theta*Smu2_s_sum;
      Seta6_s_i=Seta6_s_i + 0.25*delta_omega*delta_theta*Seta6_s_sum;
      Smu6_s_i=Smu6_s_i  + 0.25*delta_omega*delta_theta*Smu6_s_sum;
      Seta2_k_i=Seta2_k_i + 0.25*delta_omega*delta_theta*Seta2_k_sum;
      Smu2_k_I=Smu2_k_i  + 0.25*delta_omega*delta_theta*Smu2_k_sum;
      Seta6_k_i=Seta6_k_i + 0.25*delta_omega*delta_theta*Seta6_k_sum;
      Smu6_k_i=Smu6_k_i  + 0.25*delta_omega*delta_theta*Smu6_k_sum;
```

```
        end
      end
      %
      % RMS values
      %
      RMS_f     = sqrt(Sf_i);
      RMS_xi_s  = sqrt(Sxi_s_i);
      RMS_xi_k  = sqrt(Sxi_k_i);
      RMS_xi0_s = sqrt(Sxi0_s_i);
      RMS_xi0_k = sqrt(Sxi0_k_i);
      RMS_F2s_t = sqrt(SF2s_t_i);
      RMS_F2k_t = sqrt(SF2k_t_i);
      RMS_eta2_s= sqrt(Seta2_s_i);
      RMS_mu2_s = sqrt(Smu2_s_i);
      RMS_eta6_s= sqrt(Seta6_s_i);
      RMS_mu6_s = sqrt(Smu6_s_i);
      RMS_eta2_k= sqrt(Seta2_k_i);
      RMS_mu2_k = sqrt(Smu2_k_i);
      RMS_eta6_k= sqrt(Seta6_k_i);
      RMS_mu6_k = sqrt(Smu6_k_i);
      %
      RMS_f_vector(ibeta,iSpeed)   = RMS_f/(rho*g*L^2);
      RMS_eta2_s_vector(ibeta,iSpeed)= RMS_eta2_s/RMS_mu2_s;
      RMS_eta6_s_vector(ibeta,iSpeed)= RMS_eta6_s/RMS_mu6_s;
      RMS_eta2_k_vector(ibeta,iSpeed)= RMS_eta2_k/RMS_mu2_k;
      RMS_eta6_k_vector(ibeta,iSpeed)= RMS_eta6_k/RMS_mu6_k;
      %
      if RMS_eta2_s_vector(ibeta,iSpeed) > motion_ratio
         RMS_eta2_s_vector(ibeta,iSpeed) = motion_ratio;
      end
      if RMS_eta6_s_vector(ibeta,iSpeed) > motion_ratio
         RMS_eta6_s_vector(ibeta,iSpeed) = motion_ratio;
      end
      if RMS_eta2_k_vector(ibeta,iSpeed) > motion_ratio
         RMS_eta2_k_vector(ibeta,iSpeed) = motion_ratio;
      end
      if RMS_eta6_k_vector(ibeta,iSpeed) > motion_ratio
         RMS_eta6_k_vector(ibeta,iSpeed) = motion_ratio;
      end
   end        % Loop on beta ends
end           % Loop on speed ends
%
% Save results
%
clear msv*
clear mkv*
l_string=num2str(l);
T_m_string=num2str(T_m);
save_filename=strcat('h_speed_Bretch_',HS_string,'_',T_m_string,'_',l_string,'.mat');
save(save_filename);
```

APPENDIX E. MATLAB AMPLITUDE PLOT ALGORITHM

```
%
% Contour plots - Bretchneider short crested seas
%
type=input('Plot type (1=Speed/heading) (2=Waveheight/heading) = ');
%
% Speed-Heading plots
%
if type==1
   HS  =input('Significant Wave Height (feet) = ');
   T_m =input('Modal Period (sec) = ');
   l   =input('Length (l/L)  = ');
   HS_string=num2str(HS);
   l_string=num2str(l);
   T_m_string=num2str(T_m);
   %
   % Horizontal plane
   %
   load_filename=strcat('h_speed_Bretch_',HS_string,'_',T_m_string,'_',l_string,'.mat');
   load(load_filename);
   %
   figure(1)
   [th,r]=meshgrid((0:beta_incr:360)*pi/180,0:1:20);
   [X,Y]=pol2cart(th,r);
   h=polar(th,r);delete(h);
   hold on
   c_p=[0.000:0.005:1.0];
   contour(X',Y',RMS_f_vector,c_p),colorbar
   title('Transverse Connection Force')
   %
   figure(2)
   [th,r]=meshgrid((0:beta_incr:360)*pi/180,0:1:20);
   [X,Y]=pol2cart(th,r);
   h=polar(th,r);delete(h);
   hold on
   c_p=[0.000:0.010:motion_ratio];
   contour(X',Y',RMS_eta2_s_vector,c_p),caxis([0 motion_ratio]),colorbar
   title('Leading Ship, Sway')
   %
   figure(3)
   [th,r]=meshgrid((0:beta_incr:360)*pi/180,0:1:20);
   [X,Y]=pol2cart(th,r);
   h=polar(th,r);delete(h);
   hold on
   c_p=[0.000:0.010:motion_ratio];
   contour(X',Y',RMS_eta6_s_vector,c_p),caxis([0 motion_ratio]),colorbar
   title('Leading Ship, Yaw')
   %
   figure(4)
   [th,r]=meshgrid((0:beta_incr:360)*pi/180,0:1:20);
   [X,Y]=pol2cart(th,r);
```

```
h=polar(th,r);delete(h);
hold on
c_p=[0.000:0.010:motion_ratio];
contour(X',Y',RMS_eta2_k_vector,c_p),caxis([0 motion_ratio]),colorbar
title('Trailing Ship, Sway')
%
figure(5)
[th,r]=meshgrid((0:beta_incr:360)*pi/180,0:1:20);
[X,Y]=pol2cart(th,r);
h=polar(th,r);delete(h);
hold on
c_p=[0.000:0.010:motion_ratio];
contour(X',Y',RMS_eta6_k_vector,c_p),caxis([0 motion_ratio]),colorbar
title('Trailing Ship, Yaw')
%
% Vertical plane
%
load_filename=strcat('v_speed_Bretch_',HS_string,'_',T_m_string,'_',l_string,'.mat');
load(load_filename);
%
figure(6)
[th,r]=meshgrid((0:beta_incr:360)*pi/180,0:1:20);
[X,Y]=pol2cart(th,r);
h=polar(th,r);delete(h);
hold on
c_p=[0.000:0.005:1.0];
contour(X',Y',RMS_f_vector,c_p),colorbar
title('Vertical Connection Force')
%
figure(7)
[th,r]=meshgrid((0:beta_incr:360)*pi/180,0:1:20);
[X,Y]=pol2cart(th,r);
h=polar(th,r);delete(h);
hold on
c_p=[0.000:0.010:motion_ratio];
contour(X',Y',RMS_eta3_s_vector,c_p),caxis([0 motion_ratio]),colorbar
title('Leading Ship, Heave')
%
figure(8)
[th,r]=meshgrid((0:beta_incr:360)*pi/180,0:1:20);
[X,Y]=pol2cart(th,r);
h=polar(th,r);delete(h);
hold on
c_p=[0.000:0.010:motion_ratio];
contour(X',Y',RMS_eta5_s_vector,c_p),caxis([0 motion_ratio]),colorbar
title('Leading Ship, Pitch')
%
figure(9)
[th,r]=meshgrid((0:beta_incr:360)*pi/180,0:1:20);
[X,Y]=pol2cart(th,r);
h=polar(th,r);delete(h);
hold on
c_p=[0.000:0.010:motion_ratio];
```

```
    contour(X',Y',RMS_eta3_k_vector,c_p),caxis([0 motion_ratio]),colorbar
    title('Trailing Ship, Heave')
    %
    figure(10)
    [th,r]=meshgrid((0:beta_incr:360)*pi/180,0:1:20);
    [X,Y]=pol2cart(th,r);
    h=polar(th,r);delete(h);
    hold on
    c_p=[0.000:0.010:motion_ratio];
    contour(X',Y',RMS_eta5_k_vector,c_p),caxis([0 motion_ratio]),colorbar
    title('Trailing Ship, Pitch')
end
if type==2
    V   =input('Speed (knots) = ');
    T_m =input('Modal Period (sec) = ');
    l   =input('Length (l/L)  = ');
    V_string=num2str(V);
    l_string=num2str(l);
    T_m_string=num2str(T_m);
    %
    % Horizontal plane
    %
    load_filename=strcat('h_waveheight_Bretch_',V_string,'_',T_m_string,'_',l_string,'.mat');
    load(load_filename);
    %
    figure(1)
    [th,r]=meshgrid((0:beta_incr:360)*pi/180,0.5:0.5:30);
    [X,Y]=pol2cart(th,r);
    h=polar(th,r);delete(h);
    hold on
    c_p=[0.000:0.005:1.0];
    contour(X',Y',RMS_f_vector,c_p),colorbar
    title('Transverse Connection Force')
    %
    figure(2)
    [th,r]=meshgrid((0:beta_incr:360)*pi/180,0.5:0.5:30);
    [X,Y]=pol2cart(th,r);
    h=polar(th,r);delete(h);
    hold on
    c_p=[0.000:0.010:motion_ratio];
    contour(X',Y',RMS_eta2_s_vector,c_p),caxis([0 motion_ratio]),colorbar
    title('Leading Ship, Sway')
    %
    figure(3)
    [th,r]=meshgrid((0:beta_incr:360)*pi/180,0.5:0.5:30);
    [X,Y]=pol2cart(th,r);
    h=polar(th,r);delete(h);
    hold on
    c_p=[0.000:0.010:motion_ratio];
    contour(X',Y',RMS_eta6_s_vector,c_p),caxis([0 motion_ratio]),colorbar
    title('Leading Ship, Yaw')
    %
    figure(4)
```

```
[th,r]=meshgrid((0:beta_incr:360)*pi/180,0.5:0.5:30);
[X,Y]=pol2cart(th,r);
h=polar(th,r);delete(h);
hold on
c_p=[0.000:0.010:motion_ratio];
contour(X',Y',RMS_eta2_k_vector,c_p),caxis([0 motion_ratio]),colorbar
title('Trailing Ship, Sway')
%
figure(5)
[th,r]=meshgrid((0:beta_incr:360)*pi/180,0.5:0.5:30);
[X,Y]=pol2cart(th,r);
h=polar(th,r);delete(h);
hold on
c_p=[0.000:0.010:motion_ratio];
contour(X',Y',RMS_eta6_k_vector,c_p),caxis([0 motion_ratio]),colorbar
title('Trailing Ship, Yaw')
%
% Vertical plane
%
load_filename=strcat('v_waveheight_Bretch_',V_string,'_',T_m_string,'_',l_string,'.mat');
load(load_filename);
%
figure(6)
[th,r]=meshgrid((0:beta_incr:360)*pi/180,0.5:0.5:30);
[X,Y]=pol2cart(th,r);
h=polar(th,r);delete(h);
hold on
c_p=[0.000:0.005:1.0];
contour(X',Y',RMS_f_vector,c_p),colorbar
title('Vertical Connection Force')
%
figure(7)
[th,r]=meshgrid((0:beta_incr:360)*pi/180,0.5:0.5:30);
[X,Y]=pol2cart(th,r);
h=polar(th,r);delete(h);
hold on
c_p=[0.000:0.010:motion_ratio];
contour(X',Y',RMS_eta3_s_vector,c_p),caxis([0 motion_ratio]),colorbar
title('Leading Ship, Heave')
%
figure(8)
[th,r]=meshgrid((0:beta_incr:360)*pi/180,0.5:0.5:30);
[X,Y]=pol2cart(th,r);
h=polar(th,r);delete(h);
hold on
c_p=[0.000:0.010:motion_ratio];
contour(X',Y',RMS_eta5_s_vector,c_p),caxis([0 motion_ratio]),colorbar
title('Leading Ship, Pitch')
%
figure(9)
[th,r]=meshgrid((0:beta_incr:360)*pi/180,0.5:0.5:30);
[X,Y]=pol2cart(th,r);
h=polar(th,r);delete(h);
```

```
    hold on
    c_p=[0.000:0.010:motion_ratio];
    contour(X',Y',RMS_eta2_k_vector,c_p),caxis([0 motion_ratio]),colorbar
    title('Trailing Ship, Heave')
    %
    figure(10)
    [th,r]=meshgrid((0:beta_incr:360)*pi/180,0.5:0.5:30);
    [X,Y]=pol2cart(th,r);
    h=polar(th,r);delete(h);
    hold on
    c_p=[0.000:0.010:motion_ratio];
    contour(X',Y',RMS_eta5_k_vector,c_p),caxis([0 motion_ratio]),colorbar
    title('Trailing Ship, Pitch')
end
```

THIS PAGE INTENTIONALLY LEFT BLANK

LIST OF REFERENCES

Abkowitz, M.A. *Stability and Control of Ocean Vehicles.* MIT Press. Cambridge, MA, 1969.

Bascom, W. *Waves and Beaches.* Bantam Doubleday Dell Publishing Group, Inc. 1980.

Beck, R.F. and Cummins, W.E. *Principles of Naval Architecture*: Volume III, Chapter VIII, Section 1-3. Society of Naval Architects and Marine Engineers. Jersey City, NJ. 1989.

Beck, R. F. and Reed, A. M. "Modern Computational Methods for Ships in a Seaway." Twenty-Third Symposium on Naval Hydrodynamics. August. 2001.

Brard, Roger. "Some Notes on Interaction Effects Between Ships Close Aboard In Deep Water." David W. Taylor Naval Ship Research and Development Center. 1976.

Clayton, B.R. and Bishop, R.D. *Mechanics of Marine Vehicles.* J.W. Arrowsmith Publishing. Great Britain. 1982.

Devore, J.L. *Probability and Statistics*. Duxbury. Pacific Grove, CA. 2000.

Garrison, C.J. "Application of Slender Body Theory in Ship Hydrodynamics at High-Froude Number." Naval Postgraduate School. Monterey, CA. May. 1977.

Gertler, Morton. *First Symposium On Ship Maneuverability.* David Taylor Model Basin. 1960.

Gokce, M. "Coupled Stability Analysis of Close Proximity Ship Towing." Naval Postgraduate School. Monterey, CA. March. 2002.

Heald, M.A. and Elmore, W.C. *Physics of Waves*. Dover Publications, Inc. New York, NY. 1969.

Korsmeyer, T. and Kring, D. "Coupling Structural and Hydrodynamic Analyses." December. 1998.

McCreight, K.K. "A Note on the Selection of Wave Spectra for Design Evaluation." Naval Surface Warfare Center. January. 1998.

Nash, C. "Vertical Plane Response of Surface Ships in Close Proximity Towing." Naval Postgraduate School. Monterey, CA. June. 2001.

Newman, J.N. *Marine Hydrodynamics*. MIT Press. Cambridge, MA, 1977.

Ochi, M.K. *Ocean Waves: The Stochastic Approach*. Cambridge University Press. London. 1998.

Ohkusu, M. *Advances In Marine Hydrodynamics*. Computational Mechanics Publications. Boston, MA. 1996.

Orhan, O. "Design Procedure For Seakeeping Analysis of Close Proximity Ship Towing." Naval Postgraduate School. Monterey, CA. March. 2002.

Oossanen, P.V. and Manen, J.D. *Principles of Naval Architecture*: Volume II, Chapter V, Section 1-9. Society of Naval Architects and Marine Engineers. Jersey City, NJ. 1988.

Price, W.G. and Bishop, R.D. *Probabilistic Theory of Ship Dynamics*. John Wiley. 1976.

Price, W.G. and Bishop, R.D. *Hydroelasticity of Ships.* Cambridge University Press. London. 1979.

Rodriquez, R. "A Characterization of Sway Forces Induced by Close Proximity Ship Towing." Naval Postgraduate School. Monterey, CA. March. 2002.

Shin, Y.S. and Chen, H.H. "Correlation of Theoretical and Measured Hydrodynamic Pressures for the SL-7 Containership and the Great Lakes Bulk Carrier S.J. Cort." USCG Office of Merchant Marine Safety. Washington, D.C. 1983

Total Ship Systems Engineering (TSSE). "Sea Lance Littoral Warfare Small Combatant System." Naval Postgraduate School. Monterey, CA. January. 2001

Tuck, E.O. "Wave Resistance of Thin Ships and Catamarans." University of Adelaide. January. 1987.

Varyani, K.S. "Effect of Forward Speed On 2D Surface Piercing Body." University of Glasgow. London

Wu, G.X. and Taylor, R.E. "The Numerical Solution of the Motions of a Ship Advancing in Waves." University College of London. London.

Yang, C. Noblesse, F. Lohner, R. and Hendrix, D. "Practical CFD Applications to Design of a Wave Cancellation Multihull Ship." George Mason University. 2001.

Mark 4:35-41. *The Holy Bible: New International Version*. Zondervan Publishing House. Grand Rapids, MI. 1984.

INITIAL DISTRIBUTION LIST

1. Defense Technical Information Center
   Fort Belvoir, Virginia

2. Dudley Knox Library
   Naval Postgraduate School
   Monterey, California

3. Professor Papoulias
   Naval Postgraduate School
   Monterey, California

4. ENS Carol Graeber
   U.S. Coast Guard Headquarters
   Washington, D.C.

5. P.A. Wittmann
   Fleet Numerical Meteorology and Oceanography Center
   Monterey, California